



RESEARCH ARTICLE

10.1029/2022JD037042

Key Points:

- Outside of a small (85 km) zone downwind of Chicago, ozone concentrations and production near Lake Michigan is generally NO_x-sensitive
- On event days 10% decrease in volatile organic compound emission can lower MDA8 by 0.4% and 10% decrease in nitrogen oxides emission can lower MDA8 by 0.8% over Lake Michigan
- Volatile chemical product emissions were modeled to produce an average 2.7 ppb ozone increase over the lake

Supporting Information:

Supporting Information may be found in the online version of this article.

Correspondence to:

M. Abdi-Oskouei,
maryamao@ucar.edu

Citation:

Abdi-Oskouei, M., Roozitalab, B., Stanier, C. O., Christiansen, M., Pfister, G., Pierce, R. B., et al. (2022). The impact of volatile chemical products, other VOCs, and NO_x on peak ozone in the Lake Michigan region. *Journal of Geophysical Research: Atmospheres*, 127, e2022JD037042. <https://doi.org/10.1029/2022JD037042>

Received 29 APR 2022

Accepted 21 OCT 2022

The Impact of Volatile Chemical Products, Other VOCs, and NO_x on Peak Ozone in the Lake Michigan Region

Maryam Abdi-Oskouei^{1,2} , Behrooz Roozitalab^{1,2,3} , Charles O. Stanier^{2,3,4} , Megan Christiansen^{2,3,4} , Gabriele Pfister⁵ , R. Bradley Pierce⁶, Brian C. McDonald⁷, Zac Adelman⁸, Mark Janseen⁸, Angela F. Dickens⁸, and Gregory R. Carmichael^{2,3}

¹University Corporation for Atmospheric Research (UCAR), Boulder, CO, USA, ²Center for Global and Regional Environmental Research (CGRER), University of Iowa, Iowa City, IA, USA, ³Chemical and Biochemical Engineering, University of Iowa, Iowa City, IA, USA, ⁴IIHR Hydroscience and Engineering, University of Iowa, Iowa City, IA, USA, ⁵National Center for Atmospheric Research (NCAR), Boulder, CO, USA, ⁶Space Science and Engineering Center, University of Wisconsin, Madison, WI, USA, ⁷National Oceanic and Atmospheric Administration (NOAA) Chemical Sciences Laboratory, Boulder, CO, USA, ⁸Lake Michigan Air Directors Consortium (LADCO), Hillside, IL, USA

Abstract High concentrations of ozone along the coastline of Lake Michigan are a persistent air quality management challenge. Complementing observations during the 2017 Lake Michigan Ozone Study (LMOS 2017), WRF-Chem modeling was used to quantify sensitivity of modeled ozone (O₃) to anthropogenic nitrogen oxides (NO_x) and volatile organic compound (VOC) emissions, including to changes in volatile chemical product (VCP). The daily maximum 8 hr average (MDA8) over the high ozone region of Lake Michigan decreased by 2.7 ppb with exclusion of VCP from the inventory, and was sensitive to both NO_x and VOC changes, with greater sensitivity to NO_x. Close to urban centers, MDA8 ozone was VOC-sensitive. Clusters of coastal receptor sites were identified based on similarity in response to emission perturbations, with most clusters being NO_x-sensitive and NO_x-sensitivity increasing with distance from major emission sources. The 2 June 2017 ozone event, which has received considerable focus, is shown to be atypical due to unusually strong and spatially extended VOC-sensitive behavior. WRF-Chem integrated reaction rate analysis was used to compute radical termination rates due to NO_x (LNO_x) and to radical-radical reactions (LRO_x). LRO_x/LNO_x and formaldehyde to NO₂ ratio (FNR) were shown to be predictive of modeled MDA8 ozone sensitivity, but with variation in predictive power as a function of time of day, which has implications for air quality management use of FNR from geostationary satellites.

Plain Language Summary Surface ozone is an air pollutant of concern due to human health impacts. In locations with elevated ozone concentrations, including coastal regions around Lake Michigan, ozone pollution is managed by controlling emissions of the two classes of chemicals that drive ozone chemistry: volatile organic compounds (VOCs) and nitrogen oxides (NO_x). However, due to large reductions in emissions of NO_x and VOC over the past 20 years, the leverage that future reductions will have is uncertain. Reductions of 4–5 ppb (~7%) are needed in several locations, relative to 2017–2019 concentrations, to meet the 2015 ozone standard of 70 ppb. In this paper, we use simulations of atmospheric chemistry and airflow over the Midwestern US to address this issue. By comparing simulations based on different VOC and NO_x emissions, we find that reductions in NO_x emissions have more influence on ozone than reductions in VOC emissions, except for a small zone downwind of Chicago. On high ozone days over Lake Michigan, a 10% decrease in VOC (NO_x) emissions can lower ozone in the key high ozone zone over southern Lake Michigan by 0.4% (0.8%). Volatile chemical products, an uncertain component of emission inventories, are responsible for 2.7 ppb (~4%) of ozone.

1. Introduction

The Lake Michigan Ozone Study conducted in 2017 (Stanier et al., 2021) was a multi-site collaborative field campaign to support atmospheric chemistry studies and air quality management in the Lake Michigan region. While peak ozone concentrations in the region have fallen in response to ozone precursor emission reductions, ambient air quality requirements have grown stricter over the same period. For example, ozone at lakeshore Wisconsin monitors has fallen from 100 to 75 ppb from 2001 to 2020 (WDNR, 2021). Thus, coastal portions of Wisconsin, Illinois, Indiana, and Michigan do not meet the 2015 National Ambient Air Quality Standards for

© 2022 The Authors.

This is an open access article under the terms of the [Creative Commons Attribution-NonCommercial License](#), which permits use, distribution and reproduction in any medium, provided the original work is properly cited and is not used for commercial purposes.

ozone (United States Environmental Protection Agency (U. S. EPA) 2021). One of the key objectives of LMOS 2017 was update to estimates of sensitivity of ozone to its precursors, volatile organic compounds (VOCs) and nitrogen oxides ($\text{NO}_x = \text{NO} + \text{NO}_2$), using updated emission inventories and high-resolution well-characterized photochemical grid models (PGMs). As shown below, existing estimates of the sensitivity of peak ozone to emissions are outdated given the “moving target” of decreasing emissions. NO_x emissions decreases are especially large, dropping by 62% between 1997 and 2017 (Stanier et al., 2021) in inventories across EPA Region V (consisting of Illinois, Indiana, Michigan, Minnesota, Ohio, and Wisconsin). In addition to updating emission sensitivities using new emissions, the LMOS 2017 team sought to quantify the impact of volatile chemical products (VCPs) in the region, and integrate observed chemical indicators of ozone sensitivity into analysis—including indicators measured during LMOS 2017, and indicators that are increasingly available through satellite remote sensing and through future field studies.

Of recent interest is the sensitivity of air quality to VCPs which include pesticides, coatings, printing inks, adhesives, cleaning agents, and personal care products. VCPs are a major contributor to VOC reactivity in urban areas now that industrial and tailpipe emissions have been reduced (McDonald, de Gouw, et al., 2018). Areas of active investigation with respect to VCP include their oxidation chemistry, ozone formation potential, secondary organic aerosol formation potential, quantity and timing of emissions, and representation in inventories and chemical mechanisms. As Qin et al. (2021) has shown, due to the ground-level release of most VCP in high population density locations, there are likely synergies in managing exposures to primary emissions and to secondary air pollutants generated from VCP. Qin et al. (2021), using the Community Multiscale Air Quality modeling system (CMAQ), showed a change in Los Angeles summertime 8-hr daily maximum (MDA8) ozone of 9 ppb with exclusion of VCP emissions. Coggon et al. (2021), using WRF-Chem for high ozone days in New York City during 2018, modeled the MDA8 ozone sensitivity to zeroing out of VCP as ranging from 5 to 12 ppb at its spatial maximum, which typically occurred about ~50 km downwind of Manhattan. To our knowledge, no estimates of sensitivity of air quality to VCP downwind of Chicago have been published.

Prior work on ozone sensitivity relevant to the Lake Michigan region can be divided into three categories: (a) older sensitivity studies, dating prior to 2005; (b) recent regionally focused sensitivity studies; and (c) national or North American studies that report on ozone sensitivity in the Great Lakes region. We review the second category here due to its highest relevance to our work. Locations are typically classified using terminology of NO_x -sensitive and VOC-sensitive regimes, with an intermediate transitional regime where sensitivity to NO_x and VOC is balanced (Sillman, 1995). In the literature, sensitivity may refer to the sensitivity of instantaneous net production (P_{O_3}) of odd oxygen ($\text{O}_x = \text{O}_3 + \text{NO}_2$), commonly defined as P_{O_3} , to changes in emissions or concentrations of ozone precursors; however, it may refer to the sensitivity of ozone mixing ratios (or their averages in time, such as MDA8) to changes in emissions or concentrations of ozone precursors. Both types of analysis are employed in this paper.

Vermeuel et al. (2019) ran a Lagrangian parcel model in F0AM (Wolfe et al., 2016) using the National Emission Inventory (NEI) 2014 at 12 km resolution with a detailed gas-phase chemical mechanism. Parcels subjected to analysis originated within the Chicago metropolitan area and terminated at an LMOS 2017 observation site 67 km north of Chicago in Zion, Illinois. Vermeuel et al. (2019) compared modeled and observed indicator ratios for the 2 June 2017 ozone episode, and reported strong VOC sensitivity at 8 a.m. Central Standard Time in Chicago, gradually evolving to weak VOC sensitivity at the receptor. Qin et al. (2019) studied sensitivity of ozone from the CMAQ model (July 2011 simulations, NEI 2011 emissions, 4 km resolution) through perturbations of NO_x and biogenic VOCs emissions. MDA8 ozone over the Great Lake region were found to be somewhat sensitive to 50% perturbations in NO_x from on-road mobile sources and to biogenic VOCs, with sensitivities of MDA8 ozone of 0.5–3 ppb for both cases. The Lake Michigan Air Directors Consortium (LADCO) (Lake Michigan Air Directors Consortium, 2018) used Comprehensive Air quality Model with extensions (CAMx) (summer 2011 simulations, NEI 2011 emissions, 12 km resolution) to analyze a wide range of sensitivity simulations to emissions tagged by state and sector, including biogenic emissions, commercial marine vessels emissions, and wildfire emissions. Key findings were strong sensitivity of ozone at coastal Wisconsin (e.g., Sheboygan and Milwaukee) monitors to emissions originating in Illinois, and sector influences (in decreasing order of importance) of non-road mobile emissions, on-road mobile emissions, non-Electrical Generating Unit (EGU) point sources, biogenic emissions, area sources, and EGU point sources. In post-analysis work for the Lake Michigan Ozone Study, Acdan et al. (2020) evaluated formaldehyde (HCHO) to nitrogen dioxide (NO_2) or formaldehyde to NO_2 ratio (FNR) ratios from the LMOS campaign measurements, and from TROPOspheric Monitoring

Instrument (TROPOMI) for 2018 and 2019. They found that during Chicago ozone exceedances, the Chicago Metropolitan Area was VOC-sensitive, a transitional sensitivity zone existed surrounding Chicago and extends northward up the Lake Michigan shoreline to Milwaukee, the remainder of the region was NO_x -sensitive, and that the transitional sensitivity area was larger on non-ozone exceedance days and smaller on high ozone days due to variation in column formaldehyde.

Acidan et al. (2020) further expanded on the LMOS 2017 trajectory analysis of Vermeuel et al. (2019), extending the Lagrangian analysis from one episode day to five episode days. Acidan et al. (2020) developed methods for examining sensitivity based on locating ridgelines of either ozone or instantaneous ozone net production (P_{O_3}) as a function of formaldehyde, NO_2 , peroxide and nitric acid formation rates and concentrations, and radical termination reaction rates, allowing comparison to techniques based on these observational indicators (Duncan et al., 2010; Jin et al., 2017; Kleinman et al., 2001; Schroeder et al., 2017; Sillman, 1995). Acidan et al. (2020) found a mix of VOC-sensitive, transitional, and NO_x -sensitive regimes depending on day and method. We further discussed results from Acidan et al. (2020) with relation to this work in Results and Discussion.

Kopplitz et al. (2021) performed a national analysis, with Chicago as one of the focus areas, combining day-of-week (DOW) observational analysis with 12-km CAMx higher order decoupled direct method model sensitivities. Two full calendar years were modeled (2007 and 2016). They note increasing NO_x -sensitivity, with weekday ozone concentrations exceed weekend values in both years (significantly in 2016) for the whole Chicago area (16 monitors). A small urban core of VOC-sensitive (NO_x -saturated) was reported, based on PGM modeling, by Kopplitz et al. (2021). They further concluded that even in regions classified as NO_x -sensitive, targeted controls on hazardous VOC compounds would have a co-benefit of exposure reduction to both ozone and air toxics.

In this paper we expand on modeling first reported in Abdi-Oskouei et al. (2020) to address the sensitivity of ozone concentration and ozone production to VCP, and to changes in VOC and NO_x emissions. The investigation is completed using recent emission inventories, and in a modeling system that is well characterized relative to LMOS 2017 chemical and meteorological measurements. We hope our work is complementary to other ozone sensitivity research in the region, which has typically focused on sensitivity at coastal receptor sites. We include such sites, but also focus on sensitivity of a high ozone region over southern lake Michigan. While measurements of this off-shore high ozone area have been sparse in the past, new field campaigns, new ship-based sampling, and satellite remote sensing are starting to turn this into an observable feature. We further expand on many prior analyses with our focus on explicit quantification of the considerable day-to-day variation in ozone episodes.

We further demonstrate that WRF-Chem's recently developed Internal Reaction Rate (IRR) tracking feature is a good tool for characterizing the variation in VOC reactivity between inventories and chemical species, and can be used to analyze net ozone production rates together with radical production and termination rates. These are used to establish the extent to which modeled and observed indicators of ozone chemical sensitivity are predictive of MDA8 ozone. This is done in anticipation of the availability of unprecedented spatiotemporal coverage of formaldehyde and NO_2 columns from geostationary satellites such as TEMPO.

2. Methods

2.1. Model Configuration

WRF-Chem version 4.0 (Grell et al., 2005; Skamarock et al., 2008) was used for simulating air quality and its response to changes in emissions. We also utilized its IRR capability (Jeffries & Tonnesen, 1994) to investigate the ozone production chemistry (Pfister et al., 2019). The single 4 km domain is similar to Abdi-Oskouei et al. (2020) and covers Lake Michigan and part of the Midwest and includes 310×260 grid cells with 53 vertical levels extending to 50 hPa and 11 layers below 1 km (Figure 1). The Model for Ozone and Related chemical Tracers (MOZART) (Emmons et al., 2010) with updated monoterpenes, isoprene, and heterogeneous chemistry (Hodzic et al., 2015; Knote et al., 2014), was adopted for simulating the gas phase chemistry. The Model for Simulating Aerosol Interactions and Chemistry, developed by Zaveri et al. (2008) with updated secondary organic aerosol formation (Hodzic & Jimenez, 2011), was used for simulating aerosol chemistry and thermodynamics. The new Tropospheric Ultraviolet and Visible was used for photolysis parameterization (Atmospheric Chemistry Observation & Modeling (ACOM) 2021). Chemical initial and lateral boundary conditions were taken from the European Centre for Medium-Range Weather Forecasts Monitoring Atmospheric Composition and Climate reanalysis (Inness et al., 2013) the Copernicus Atmosphere Monitoring Service (CAMS) model. The

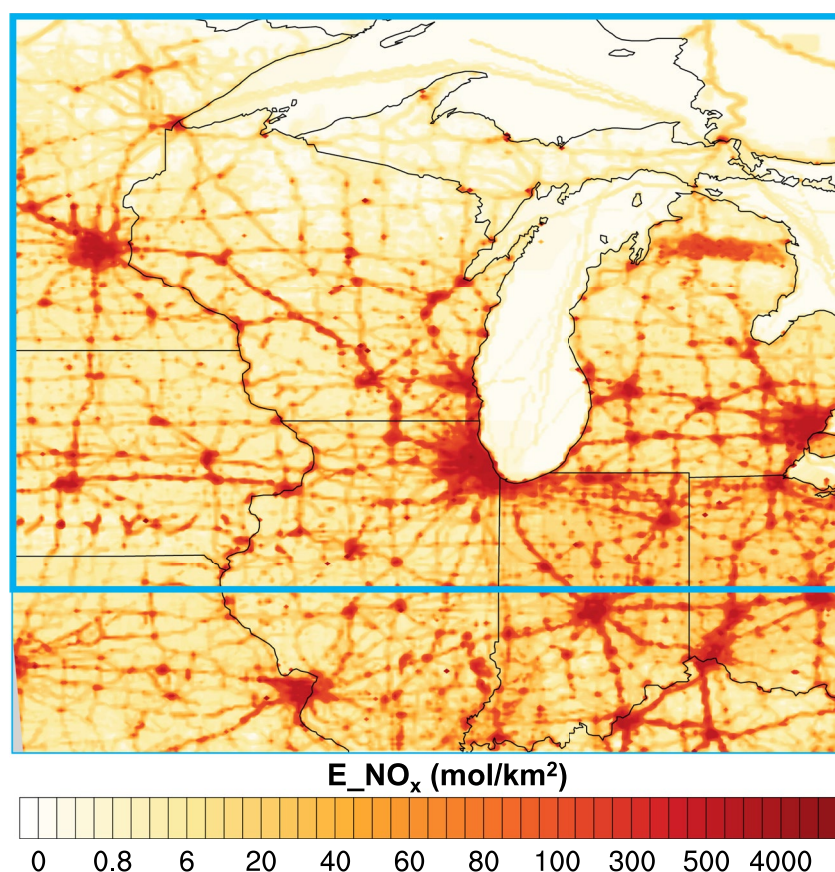


Figure 1. Modeling domain, overlaid with anthropogenic NO_x emissions from NEI17. The blue box shows the averaging area used for reported emission rates.

3 km High-Resolution Rapid Refresh (HRRR) model (Benjamin et al., 2016) provided meteorological boundary conditions. Abdi-Oskouei et al. (2020) showed that HRRR data led to better meteorological results compared with the National Center for Environmental Prediction Final Analysis (NCEP-FNL) data. Following Abdi-Oskouei et al. (2020), the meteorology was reinitialized daily with HRRR data, while the chemical state was carried over from the previous day's simulation. Table S1 in Supporting Information S1 summarizes the WRF-Chem configurations options used in this study and additional details on the physical configuration properties and initialization can be found in Abdi-Oskouei et al. (2020). The modeling domain and averaging areas used for reporting integrated emissions are shown in Figure 1.

2.2. Emission Inventories and Sensitivity Simulations

The Model of Emissions of Gases and Aerosols from Nature (MEGAN v2.0.4) (Guenther et al., 2006) was used to simulate biogenic emissions online in the WRF-Chem simulations. By default, MEGAN uses monthly MODIS 2003 Leaf Area Index data to estimate biogenic emissions rates. The online MEGAN also estimates soil NO emissions. There were not any large fires in the domain during the study and fire emissions were excluded within the domain. The chemical boundary conditions from the CAMS model included out-of-domain fire emissions.

The total of five different anthropogenic emission inventories were used to perform the sensitivity simulations. Emission inventories were based on the U.S. EPA NEI for years 2011 (NEI11) and 2017 (NEI17).

We also utilize the Fuel-based Inventory for Vehicle Emissions (FIVE) and VCP (FIVE18_VCP) for mobile sources (McDonald, McKeen, et al., 2018) and VCP (McDonald, de Gouw, et al., 2018), respectively. Oil and gas sector emissions in these inventories are from the Fuel-based Oil & Gas inventory (Francoeur et al., 2021). Power plant emissions are updated with Continuous Emissions Monitoring System data. Other area and point

source emissions are taken from the NEI 2014. Herein, we refer to this inventory as the FIVE18_VCP inventory, which is gridded at $4 \text{ km} \times 4 \text{ km}$ resolution across the continental US and utilized in Coggon et al. (2021) and Li et al. (2021). Emissions outside of the US are based on those from the NEI 2005 and scaled to more recent years for Canada and Mexico using CEDS (Hoesly et al., 2016). The effects of VCP on simulated ozone formation were studied using the inventories FIVE18_VCP and FIVE18_noVCP, which were identical except for exclusion of VCP throughout the domain in the noVCP variant. Nitrogen oxides emissions from NEI11 were adjusted downward using a multiplier of 0.72 to adjust 2011 emissions to the 2017 modeling year, forming a modified (NEI11m) inventory as described in Abdi-Oskouei et al. (2020). NEI11m, FIVE18_VCP, and FIVE18_noVCP are hourly emissions averaged over the month of July. This means that there is a diurnal cycle but no day-to-day variability in these emission inventories. NEI17 (and NEI17m) is a daily emission inventory created for the LMOS campaign period and has both diurnal and day-to-day variability.

To assess the impact of changes in NO_x emission, while keeping VOC emission constant, a variant of NEI17 was used (NEI17m) consisting of a 20% anthropogenic NO_x increase. Integrated emissions from these inventories are presented in summary form in the results and discussion section. The WRF-Chem outputs used in this study are available from Abdi-Oskouei et al. (2022).

2.3. Observational Data and Evaluation Methods

Observational data was drawn from the LMOS 2017 campaign repository at NASA as described in the campaign overview (Stanier et al., 2021). Additional data was used from the U.S. EPA Air Quality System. Analysis focused primarily on 10 ozone episode days that were identified by the LMOS team and described in Doak et al. (2021). These were divided into three periods: episode A (June 2–4), episode B (June 9–12) and episode C (June 14–16).

Two groups of surface observations were utilized. One was a group of routine monitoring sites on the coastal west region of Lake Michigan. Referred to in this work as the “coastal west” grouping, it consisted of 26 sites for ozone, and 8 for NO_2 , and are consistent with the coastal west analysis area used in Abdi-Oskouei et al. (2020). The second grouping, referred to as the “receptor sites” grouping, consisted of 21 ozone monitoring stations spread over four states (WI, IL, IN, MI) around Lake Michigan. These were selected by personnel at LADCO for their historical relevance in ozone air quality management planning. Thirteen receptor sites are also in the coastal west group. Statistical analysis of MDA8 ozone and NO_2 concentrations used the metrics and benchmarks proposed in Emery et al. (2016); Qin et al. (2019).

2.4. Analysis Framework

Several complementary analyses were conducted to understand the impacts of emission changes on surface ozone concentration, explore the high ozone regions over the lake, and characterize the major VOC species contributing to ozone formation. The methods for these analyses are as follows.

The first analysis reported in the results section is the simple ozone sensitivity to emissions inventory (limited to the high ozone episode days). For example, the difference between MDA8 ozone on episode days between the FIVE18_VCP and FIVE18_noVCP shows the effect of VCP emissions on ozone episode days, and we report this as both the effect of VCP and of anthropogenic VOC. The analysis focused on four emission inventory combinations: NEI17 & NEI11m, FIVE18_VCP and NEI11m, NEI17 and NEI17m, FIVE18_noVCP and FIVE18_VCP. Together these show the effects of various combinations of NO_x and VOC emission changes. The frequent comparison to NEI11m is, in part, because this is our most widely used base case, used in forecasting for LMOS 2017, and in values reported in previous LMOS 2017 publications (Abdi-Oskouei et al., 2020; Abdioskouei et al., 2019).

In a second analysis, day-specific over-lake high ozone (OLHO) regions were identified and the analysis was restricted to them. This approach of focusing on the OLHO region in the simulation permits extraction of the modeled sensitivity in a region with high net ozone production. Due to transport errors in PGMs and limited ozone measurements over the lake, a focus only on sensitivity at locations with high *observed* ozone can be misleading. The approach of focusing on the OLHO region is supported by the conceptual model of ozone formation over Lake Michigan described in the literature (Cleary et al., 2015; Dye et al., 1995; Foley et al., 2011). In the conceptual model, ozone is produced over the lake, and then transported to coastal monitors by the lake

breeze and/or synoptic winds. This pattern was observed on many of the LMOS 2017 days. Thus, understanding emission sensitivity of ozone production and concentrations over Lake Michigan is relevant to improving conceptual understanding and air quality management policies. We believe this approach is complementary to other approaches that focus on sensitivities at receptor sites.

Identification of the OLHO region was as follows. In the southern portion of Lake Michigan (defined as below 45°N), the 20% of grid cells over water with the highest surface MDA8 ozone were identified for each emission inventory and each of the 10 episode days (shown in Figures S1–S3 in Supporting Information S1). For each episode day, the intersection of high ozone regions in the four simulations is used to form a consistent set of high ozone grid cells, referred to as the day-specific over-lake high ozone (OLHO) region. For the related variables that we analyze in conjunction with MDA8 ozone variables (e.g., NO_x concentrations), the average from 1000 to 1400 LST at the same locations was used, consistent with the approach of Pusede and Cohen (2012). Throughout this work, temporal averages are from 1000 to 1400 LST unless otherwise specified.

With identical NO_x emissions and nearly identical NO₂ concentrations in the OLHO region for the FIVE18_VCP and FIVE18_noVCP emission cases, a VOC sensitivity S_{VOC} was

$$S_{\text{VOC}} = \frac{\langle C_{\text{O}_3} \rangle_{\text{VCP}} - \langle C_{\text{O}_3} \rangle_{\text{noVCP}}}{\langle C_{\text{VOC}} \rangle_{\text{VCP}} - \langle C_{\text{VOC}} \rangle_{\text{noVCP}}} \quad (1)$$

where the angle bracket indicates the mean concentration of the OLHO grid cells on a given day. A sensitivity to changes in NO₂ was calculated in a similar fashion using two runs with a difference in anthropogenic NO_x emissions, but with identical VOC emissions,

$$S_{\text{NO}_x} = \frac{\langle C_{\text{O}_3} \rangle_{\text{NEI17m}} - \langle C_{\text{O}_3} \rangle_{\text{NEI17}}}{\langle C_{\text{NO}_x} \rangle_{\text{NEI17m}} - \langle C_{\text{NO}_x} \rangle_{\text{NEI17}}} \quad (2)$$

where the NEI17m emission inventory is NEI17 with a 20% NO_x increase, uniformly applied to all sectors.

A third group of analyses used the IRR capability of WRF-Chem to investigate ozone formation and ozone sensitivity in the region outlined in Figure 4 maps, and more broadly across the modeling domain. The IRR module provides the accumulative hourly reaction amount for all the reactions in the MOZART gas phase mechanism (Pfister et al., 2019). This capability was specifically used to investigate the compounds contributing to the VOC reactivity over the southern portion of Lake Michigan, and to compute LRO_x/LNO_x over the domain. LNO_x and LRO_x are the rates of all pathways destroying HO_x (OH, HO₂, and RO₂) through NO_x, and through other radical-radical reactions (e.g., RO₂ + RO₂), respectively. The reactions considered in the LRO_x and LNO_x can be found in Tables S2 and S3 in Supporting Information S1. The ratio is calculated within the planetary boundary layer to minimize mixing errors (Pfister et al., 2019). Because HO_x cycling is critical to ozone production, the dominant HO_x termination pathway has been used as an indicator of ozone sensitivity. Termination by radicals (LRO_x) is dominant in a NO_x-sensitive regime, while radical loss termination by NO_x (LNO_x) is dominant in a VOC-sensitive regime. While the LRO_x/LNO_x ratio of 1 was previously considered as the transition point, Schroeder et al. (2017) found that the ozone production rates peak at a ratio of 0.35, due to growth in the overall radical pool as NO_x is increased from LRO_x/LNO_x of 1 to LRO_x/LNO_x of 0.35; therefore, LRO_x/LNO_x of 0.35 is used in this work as the policy-relevant transition between VOC-sensitive (LRO_x/LNO_x < 0.35) and NO_x-sensitive (LRO_x/LNO_x > 0.35) conditions.

While LRO_x/LNO_x and FNR have been shown to be predictive of instantaneous ozone production sensitivity to concentration changes, it remains to be seen how predictive these ratios are of the more complex statistic of MDA8 ozone in a domain with complex meteorology. A system to test predictive power of these instantaneous indicator ratios to changes in MDA8 ozone is shown in Figure 2. The flow is focused on answering two questions, shown in Figure 2a as Q1 and Q2. Question 1 (Q1) is stated as, is LRO_x/LNO_x predictive of brute force sensitivity to emissions changes on ozone episode days; and if so, at what time of day is LRO_x/LNO_x most predictive? Question 2 (Q2) is the identical question but with FNR as the predictor.

As shown in Figure 2a, paired model runs are used to calculate fractional changes of MDA8 surface ozone resulting from a VOC emissions perturbation ($\Delta\text{MDA8}_{\text{voc}}$) and NO_x emissions perturbation ($\Delta\text{MDA8}_{\text{NO}_x}$). This is done separately for each day and each model grid cell, using Equations 3 and 4, respectively. The dominator represents the mean of two values.

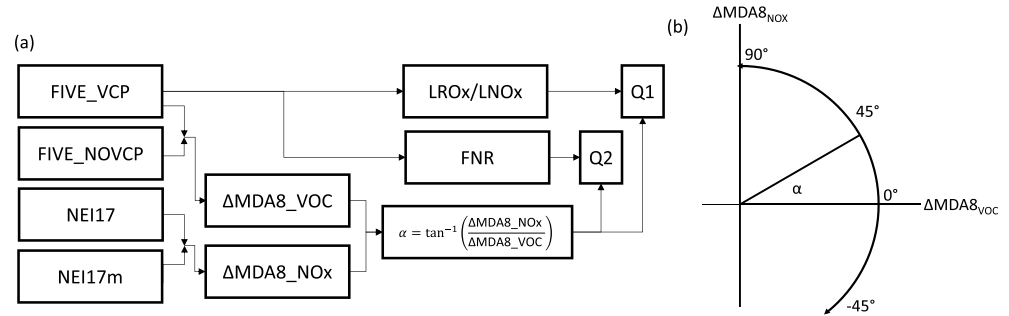


Figure 2. Graphical technique for comparing brute force model sensitivities for MDA8 surface ozone to hour- and pixel-specific LRO_x/LNO_x and FNR ratios. (a) Schematic of how the fractional change of MDA8 ozone with respect to volatile organic compound (VOC) and NO_x is predicted using four forward model runs; the FNR is computed from one forward model run; the LRO_x/LNO_x ratio is computed from one forward model run with IRR. As shown in (b) the angle that ΔMDA8_{VOC} and ΔMDA8_{NOx} make on the Cartesian plane forms a continuous variable of sensitivity to emissions, with α of 90° as NO_x-sensitive and VOC-insensitive, and 0° as NO_x-insensitive and VOC-sensitive.

$$\Delta \text{MDA8}_{\text{VOC}} = \frac{(\text{MDA8}_{\text{FIVE18-VCP}} - \text{MDA8}_{\text{FIVE18-noVCP}})}{< \text{MDA8}_{\text{FIVE18-VCP}}, \text{MDA8}_{\text{FIVE18-noVCP}} >} \quad (3)$$

$$\Delta \text{MDA8}_{\text{NOx}} = \frac{(\text{MDA8}_{\text{NEI17m}} - \text{MDA8}_{\text{NEI17}})}{< \text{MDA8}_{\text{NEI17m}}, \text{MDA8}_{\text{NEI17}} >} \quad (4)$$

The LRO_x/LNO_x and FNR ratios in the analysis are taken from the FIVE18_VCP scenario. The angle α formed by placing ΔMDA8_{VOC} and ΔMDA8_{NOx} on a Cartesian plan is used as a continuous variable of sensitivity to emissions, with α of 90° as NO_x-sensitive and VOC-insensitive, 0° as NO_x-insensitive and VOC-sensitive, and <0° as VOC-sensitive. Predictability of brute-force sensitivity to emissions (as captured by α) is assessed by the coefficient of determination (R²) of the linear regression of LRO_x/LNO_x (and FNR) versus α. Angles in the range −22.5°–112.5° were used based on visual inspection of the relationships and excessive scatter outside of those angles. Points outside those angles are probably dominated by processes other than emissions sensitivity (e.g., complex transport patterns, mixing of airmasses with different sensitivity, temporal variation in sensitivity, etc.). Also, points with a distance to the origin less than 0.05 (small fractional sensitivity to emissions) were excluded. These points are mostly further from the major emission sources and are located over land (not shown).

In a final analysis, the modeled behavior at the 21 receptor sites was grouped into spatial clusters, and behavior within each cluster was compared to behavior at the OLHO. With four emission inventories and 10 episode days, an array of 40 MDA8 ozone concentrations was available for each of the 21 sites. These sites were grouped into eight clusters using k-means cluster analysis (MATLAB kmeans function (Vassilvitskii & Arthur, 2006)). The kmeans function constructs clusters to minimize the sum, over all clusters, of the within-cluster sums of point-to-cluster-centroid “distances” where distances are based on the squared difference in ozone concentrations.

Dimensionless emissions sensitivities DS_{VOC} and DS_{NOx} were calculated within each cluster on high ozone days using Equations 5 and 6, respectively,

$$\text{DS}_{\text{VOC}} = \frac{(\text{MDA8}_{\text{VCP}} - \text{MDA8}_{\text{noVCP}}) < \text{E}_{\text{VOC-VCP}}, \text{E}_{\text{VOC-noVCP}} >}{< \text{MDA8}_{\text{VCP}}, \text{MDA8}_{\text{noVCP}} > (\text{E}_{\text{VOC-VCP}} - \text{E}_{\text{VOC-noVCP}})} \quad (5)$$

$$\text{DS}_{\text{NOx}} = \frac{(\text{MDA8}_{\text{NEI17m}} - \text{MDA8}_{\text{NEI17}}) < \text{E}_{\text{NOx-NEI17m}}, \text{E}_{\text{NOx-NEI17}} >}{< \text{MDA8}_{\text{VCP}}, \text{MDA8}_{\text{noVCP}} > (\text{E}_{\text{NOxNEI17m}} - \text{E}_{\text{NOx-NEI17}})} \quad (6)$$

where concentrations are averaged within cluster across the 10 episode days prior to calculating the statistic, and the emissions and emissions changes are based on daily average anthropogenic emissions north of 40° as discussed in Section 3.1 and shown in Figure 2. Subscripts VCP and noVCP refer to FIVE18_VCP and FIVE18_noVCP, respectively.

3. Results and Discussion

We first summarize key features of the four emission inventories used in this study. We then present model skill and statistical model performance metrics. Temporally averaged sensitivity of ozone to emissions are presented next, followed by the location and sensitivity of the OLHO region over the lake. Identification of the modeled VOC species responsible for VOC reactivity are presented next, using IRR. Ozone sensitivity using the LRO_x/LNO_x and FNR instantaneous ratios are then presented. Furthermore, we investigate the hours during the day that LRO_x/LNO_x and FNR have higher correlation with MDA8 ozone and P_{O_3} changes. Finally, the sensitivity of ozone at the receptor sites is discussed and compared to that of the OLHO region using cluster analysis.

3.1. Relevant Features of Emission Inventories

Figure 3 compares and summarizes the NO_x and VOC emissions used in this study (above 40°N latitude). While the spatial patterns of emissions are very similar between all the emission inventories (Figures S4 and S5 in Supporting Information S1 show the spatial distribution of NO_x and total VOC emissions, respectively), total emissions vary. As shown in Figure 3a, NEI11m has the highest NO_x emissions of the four inventories and NEI17 has the lowest NO_x emissions vary by about a factor two. The molar weighted emissions of major VOCs are shown in Figure 3a; VOC emissions vary by about a factor of three, with FIVE18_noVCP and FIVE18_VCP having the lowest and highest values, respectively. Speciation of emissions, by molar emission rate, is shown in Figure 3c. Large alkanes group (labeled BIGALK) is the dominant emitted species in all the inventories, and ethylene (C_2H_4) and ethanol (C_2H_5OH) are major contributors in all the inventories. Notable variation between inventories includes ethane (C_2H_6), which is 4–5 times higher in NEI17 compared to the other inventories. Acetone (CH_3COCH_3), a prominent solvent in coatings and adhesives, and ethanol (C_2H_5OH), a component in cleaning and personal care products (Gkatzelis et al., 2021), are much higher in FIVE18_VCP compared to the other inventories (McDonald, de Gouw, et al., 2018).

Weighting the different VOCs by their reactivity with OH gives a slightly different picture of the inventories, as shown in Figure 3b (totals) and d (speciated). Rate constant for the reactions between each VOC species and OH are from the MOZART mechanism at standard temperature and pressure conditions. Figure 3d shows the OH-reactivity-weighted emissions for major species within all the inventories. It shows that the emissions of higher alkenes (BIGENE), BIGALK, propene (C_3H_6), and xylene (XYLENE) have the highest reactivity-weighted contribution to the inventory. On the contrary, species such as ethanol, ethane, and acetone have low reactivity with OH and thus appear less important in the reactivity-weighted emissions. As a result, Figure 3d shows that NEI11m has the largest total OH-reactivity-weighted VOC emissions compared to other inventories, while FIVE18_VCP has the largest mole-weighted VOC emissions.

3.2. Model Evaluation

Our previous model evaluation, discussed in Abdi-Oskouei et al. (2020), focused only on modeling using the NEI11m emissions; furthermore, previously reported results used a different photolysis option. Figure 4 shows surface modeled ozone and NO_2 concentrations in four simulations based on different emission inventories. Coastal west observations are also shown using the same color scale. Ozone concentrations (when averaged over the 10 high ozone days) had a maxima over the southern portion of Lake Michigan. NO_2 had high concentrations in urban centers, with the metropolitan Chicago area standing out. This was followed by Milwaukee, WI, and by Holland, MI, and smaller cities, where daytime NO_2 exceeded regional background by about 3–7 ppb. Here we summarize performance of the latest model configuration.

A summary of comparisons of the model to observations at the coastal west locations is as follows: (a) Overall, the model, in all four scenarios, was able to capture the diurnal variation of surface ozone (with acceptable performance) and NO_2 . Diurnal average shown in Figure 5, with full time period shown in Figure S7 in Supporting Information S1, and statistical performance is shown in Table 1. (b) The maximum ozone concentrations are underpredicted on some of the high ozone days. (c) NEI17 underestimates daytime and nighttime NO_2 concentrations. (d) NEI11m captured the daytime NO_2 concentrations but overestimated maximum nighttime NO_2 values. (e) FIVE18_VCP and FIVE18_noVCP predicted similar NO_2 concentrations at the location of coastal west monitors (close to emissions sources) and better captured the nighttime NO_2 values. Figure 5 highlights how the NEI17 simulation differs from the other model simulations (and from observations). The lower NO_2 concentrations in

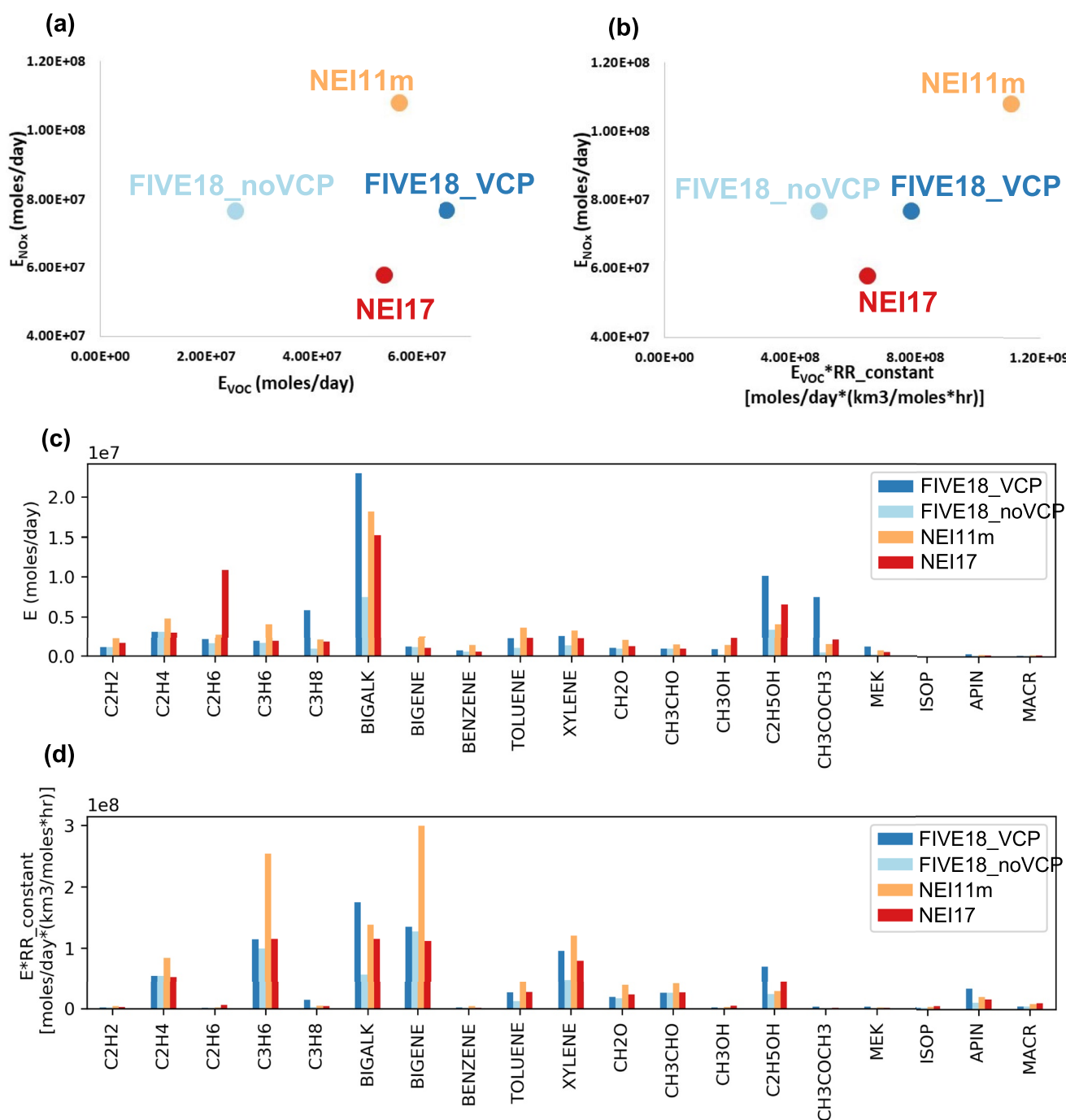


Figure 3. Emissions in the main four anthropogenic emission inventories used in this work. The NEI17m inventory is not showed as it is a simple variation to NEI17 inventory. Volatile organic compound (VOC) emissions (abscissa) versus NO_x emissions (ordinate), both north of 40° latitude, with VOC emissions weighted by (a) moles and (b) OH reactivity; major VOC emissions by their category in the Model for Ozone and Related chemical Tracers gas-phase reaction mechanism weighted by (c) moles and (d) OH reactivity. The results are for 2 June.

this simulation correspond to higher ozone concentrations at night and during the morning, and lower peak ozone concentrations during the day. Errors in the modeling system (e.g., deposition, chemistry, transport, subgrid processes, spatial representation, etc.) may offset errors in the emission inventory. Of these possible sources of error, meteorological performance was evaluated in Abdi-Oskouei et al. (2020) and found to be similar to contemporary PGMs in the region, but with inconsistent skill for representing details of the lake breeze (arrival

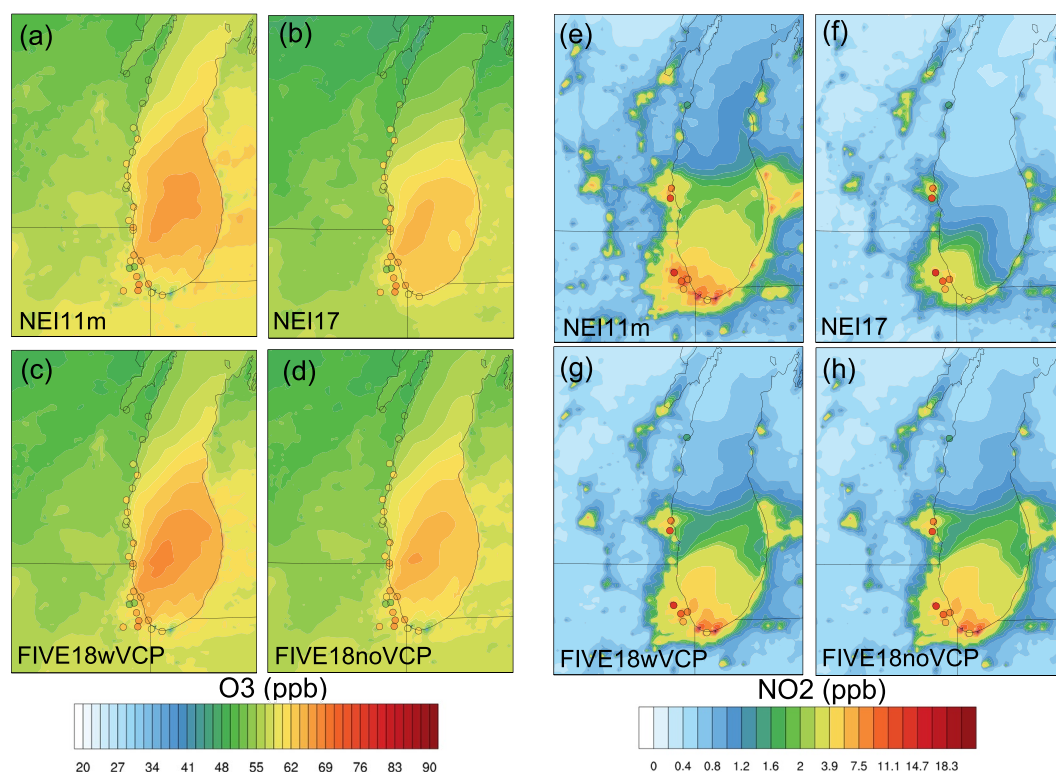


Figure 4. Daytime (09:00–17:00 LST) model mean concentrations for surface ozone (left) and surface NO_2 (right) on the 10 episode days of focus for this work. Routine monitor network measurement values overlaid as circles with same color scale. Model mean biases at the monitoring stations are displayed in Figure S6 in Supporting Information S1.

time, speed, distance of inland penetration, and vertical extent). Other potential sources of error have not been evaluated.

Statistical evaluation of MDA8 ozone from the four simulations is reported in Table 1. The upper portion of Table 1 uses all monitored MDA8 ozone values at the 26 coastal west stations on the 10 episode days. The observed mean MDA8 ozone is 63.0 ppb, compared to modeled values of 58.7–60.7 ppb, depending on the emission inventory. The performance metrics for the normalized mean error (NME) range from 5% to 7%, for the normalized mean bias (NMB) from -4 to -7% and for the correlation coefficient from 0.61 to 0.69. The correlation coefficient measures the model's ability to capture both spatial and temporal variation of MDA8 ozone across these sites and across the high ozone days. Considering the benchmarks of Emery et al. (2016), all four simulations meet the tighter (goal) benchmark for normalized mean error, and all four simulations meet the looser (criteria) benchmark for correlation coefficient. Statistical performance for the bias is within the benchmark for two cases (NEI11, FIVE18_VCP), and is close to the benchmark for the other two cases (FIVE18_noVCP and NEI17).

The lower portion of Table 1 excludes monitors with measured MDA8 ozone below 60 ppb, decreasing the size of the observation data set by 33%. In this evaluation, the mean bias (MB) increases somewhat, reflecting the higher model biases in capturing peak ozone concentrations. Although the comparison shows some shortcomings in our simulation, the statistical performance is generally similar to other recent published works. For example, Qin et al. (2019) reported (for days with MDA8 ozone observed >60 ppb), a NME of 14%–16%, which can be compared to 9%–12% in this work. For NMB, Qin et al. (2019) reported 0% to -4% , versus -9 to -12% in this work.

3.3. Overview of Sensitivity Results

Figure 6 shows the sensitivity of surface ozone concentrations to the emission inventory. As described in Section 2, the difference in MDA8 ozone is shown averaged over the 10 episode days. The effect of VCP emissions on ozone

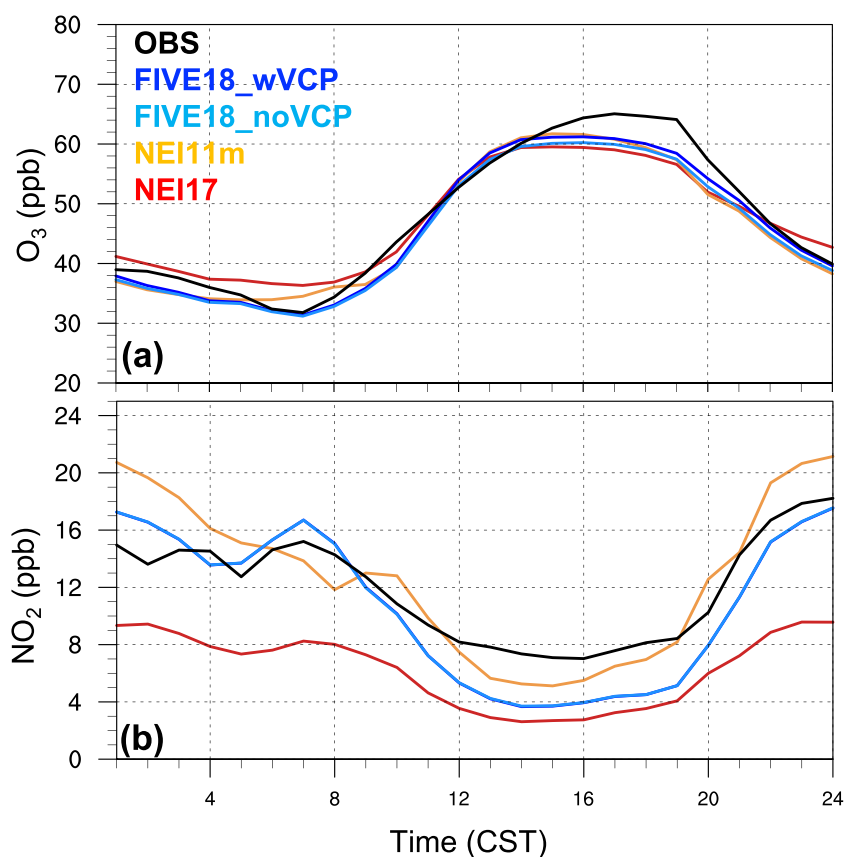


Figure 5. Diurnal pattern of (a) ozone and (b) NO₂ at monitors in the coastal west region on the 10 episode days. Figure S8 in Supporting Information S1 shows a similar plot with error bars.

Table 1

Performance Statistics for MDA8 Ozone on the 10 Episode Days of LMOS 2017

N = 260

MDA8 (ppb)	OBS	NEI11m	NEI17	FIVE18_VCP	FIVE18_noVCP	Emery goal	Emery criteria
Mean	63.03	60.65	58.66	60.47	59.39	–	–
MB	–	–2.38	–4.37	–2.57	–3.64	–	–
NMB (%)	–	–3.77	–6.93	–4.07	–5.78	<±5	<±15
NME (%)	–	4.8	7.42	5.44	6.44	<15%	<25%
<i>R</i>	–	0.69	0.62	0.69	0.61	>0.75	>0.5

N = 173

With obs > 60 ppb cut-off

MDA8 (ppb)	OBS	NEI11m	NEI17	FIVE18_VCP	FIVE18_noVCP
Mean	67.23	60.56	59.14	61.09	59.80
MB	–	–6.67	–8.1	–6.14	–7.43
NMB (%)	–	–9.92	–12.04	–9.13	–11.06
NME (%)	–	9.92	12.04	9.13	11.06
<i>R</i>	–	0.4	0.52	0.55	0.4

Note. Top section is for 26 sites and 10 days (*N* = 260). The bottom section excludes sites with observed MDA8 < 60 ppb (*N* = 173). Performance goal and criteria are from Emery et al. (2016). MB, mean bias; NMB, normalized mean bias; NME, normalized mean error.

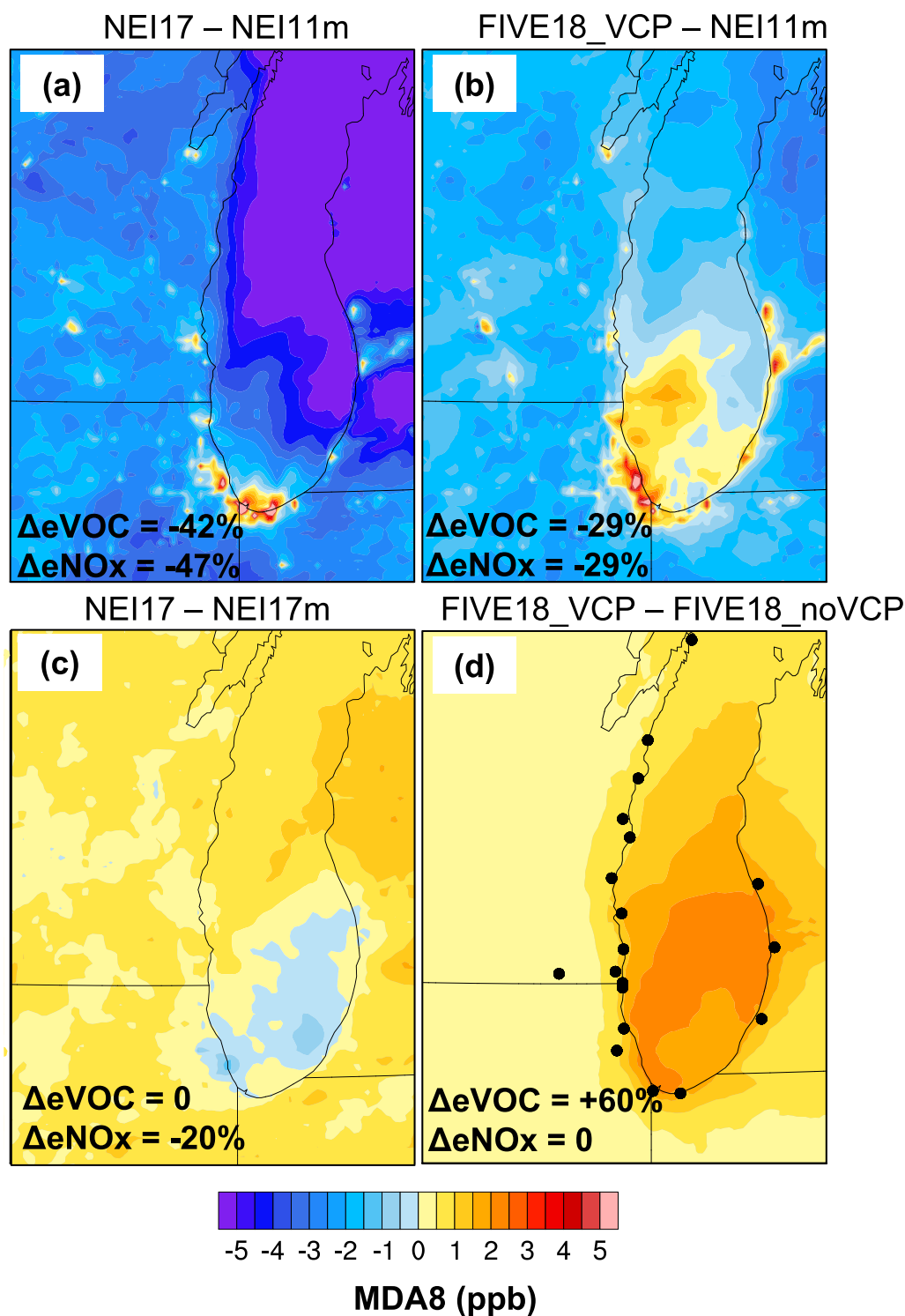


Figure 6. Sensitivity of ozone to emission changes. (a) NEI17—NEI11m; (b) FIVE18_VCP—NEI11m; (c) NEI17—NEI17m; (d) FIVE18_VCP—FIVE18_noVCP. (a, b, and c) show the effects of reductions in NO_x under various cases of changes in volatile organic compound (VOC). (d) Shows the increase in ozone attributable to the VCP portion of the inventory, under constant NO_x emissions. Black dots show the location of receptor sites. Δe shows the relative changes in OH-weighted VOC and NO_x emissions for each scenario.

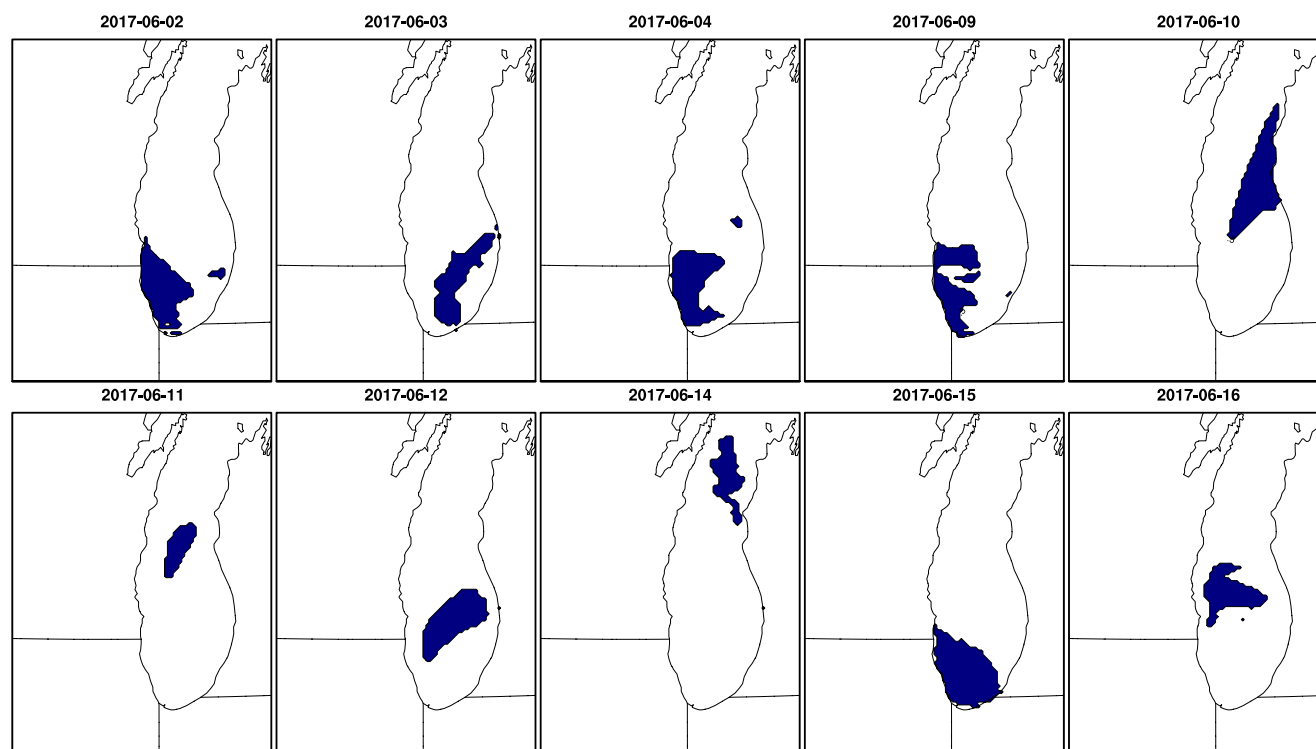


Figure 7. The 10 areas of highest modeled ozone, used for sensitivity analysis of peak over-lake MDA8 ozone to precursors.

is shown in Figure 6d, with a peak effect over the southern portion of Lake Michigan, and impact contribution of 2–2.5 ppb on the episode days averaged MDA8. Purple and blue colors, indicative of reductions in ozone mainly due to lower NO_x concentrations in rural and downwind areas that are VOC rich and NO_x -limited, are strongest in Figure 6a, which corresponds to the case with the largest NO_x emissions difference, that is, NEI17 versus NEI11m (Figure 3). Small areas of ozone increase from NO_x emission decrease (indicative of the VOC-sensitive locations) can be seen as hot spots in urban areas, particularly in Figures 6a and 6c. These can reach up to 6 ppb in the average over high ozone episode day. Average sensitivities, as shown in Figure 6, mask considerable day-to-day variability in the magnitudes and spatial patterns of modeled sensitivity.

3.4. Mid-Lake Sensitivity Estimates

Figure 7 shows the OLHO region for each episode day, determined as described in Section 2. Large areas, such as on June 2, 10, and 15, occurred when there is more consistency between spatial distribution high ozone grid cells across the four simulations. Smaller areas, such as June 11, are the result of less consistency.

Figure 8 shows the distribution of (a) MDA8 ozone, (b) VOC concentration, (c) NO_2 concentration, and (d) IRR-computed VOC sensitivity, in the areas highlighted in Figure 7, for four of the emission inventories. In addition to the individual days, the distribution of all 10 days is shown in the leftmost four boxes of Figure 8. Together, these summarize the inventory-to-inventory variation, and the day-to-day variation, in the OLHO region. To help place Figure 8 in context, we note that the average of all the MDA8 ozone data in Figure 8a is 73.0 ppb. The corresponding averages for VOC and NO_2 concentrations are 9.71 and 3.28 ppb, respectively.

Consistent with Figure 4, FIVE18_VCP (dark blue) has the highest MDA8 ozone when aggregating over the 10 days. This is followed by NEI11m (orange) and by FIVE18_noVCP (light blue); NEI17 (red) shows the lowest MDA8 ozone. This ordering of ozone concentrations by inventory is repeated on many, but not all, of the individual episode days. For example, the NEI17 inventory is not the lowest for ozone on June 2. And the FIVE18_VCP inventory is not the highest for ozone on June 3 and June 9.

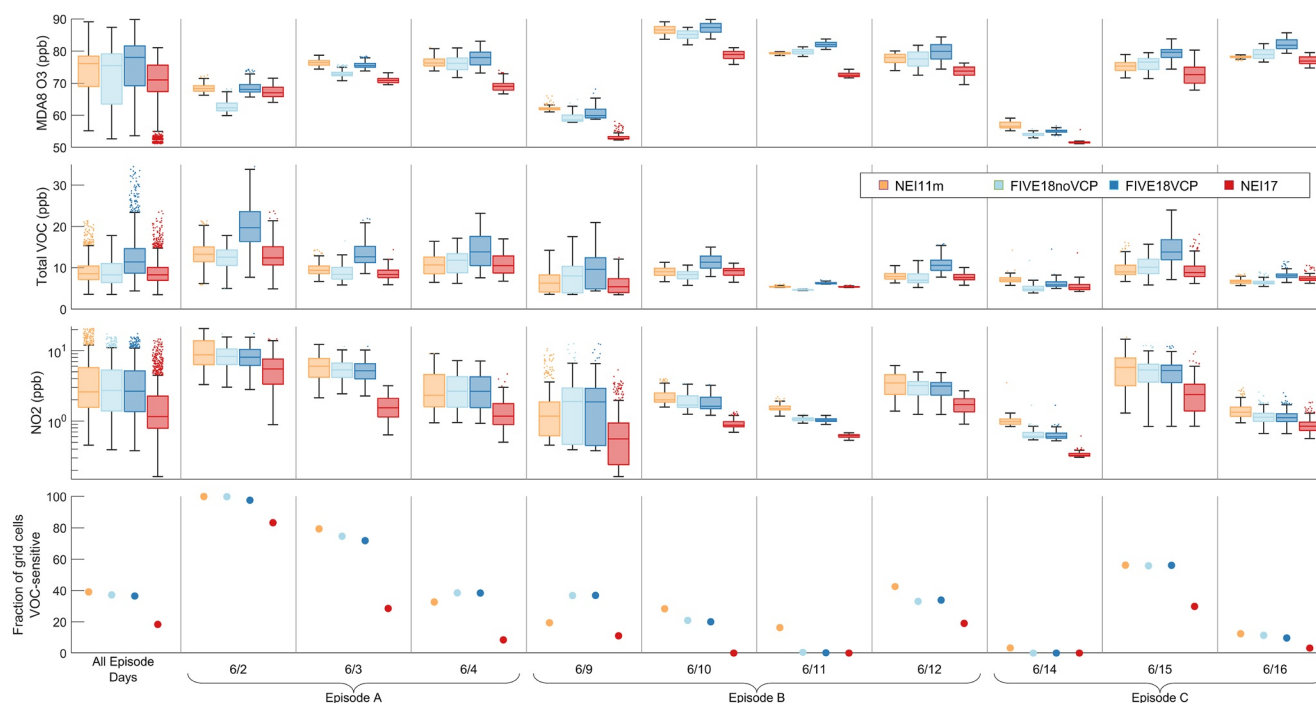


Figure 8. Boxplot of (a) MDA8 ozone, (b) volatile organic compound (VOC) and (c) NO₂ concentrations for different model simulations in the over lake high ozone region. Panel (d) shows the percent of grid cells meeting a VOC-sensitive condition using LRO_x/LNO_x. Color coding indicates the emission inventory (legend in panel b), with NEI11m as orange, FIVE18_noVCP as light blue, FIVE18_VCP as dark blue, and NEI17 as red. Ozone is MDA8 (daily) and VOC, NO₂, and LRO_x/LNO_x are from 10:00 to 14:00 LST.

Figure 8b shows the distributions of VOCs for each day and emission sensitivity case. The VOC concentrations are highest for the FIVE18_VCP case and lower (and similar) for the remaining three emission sensitivity cases. Patterns for NO₂ in Figure 8c are consistent with Figures 3–5—NO₂ is similar, on average, in all inventories except in NEI17, where it is significantly lower.

Figure 8d summarizes the IRR-based VOC versus NO_x sensitivity metric. The value plotted is the fraction of grid cells in the OLHO region that are VOC-sensitive, defined as LRO_x/LNO_x < 0.35. Low values of this metric indicate radical termination by reactions with NO_x are significantly more common than radical termination by reactions with HO₂ and RO₂ radicals. This varies by episode day, with most of the OLHO region on June 2 and 3 as VOC-sensitive and the remainder of the days having OLHO regions comprised mainly of grid cells that are NO_x-sensitive by the LRO_x/LNO_x metric. The NEI17 inventory has significantly lower VOC sensitivity than the other inventories. Unsurprisingly, the variation in the sensitivity metric (Figure 8d) follows similar patterns to the NO₂ concentrations (Figure 8c). The LRO_x/LNO_x results from IRR are discussed in greater detail below.

The results of this sensitivity estimation are shown in Table 2. As shown in the first row (“all 10 cases”), aggregating across all episode days yields a VOC sensitivity of 0.78 pb MDA8 ozone per ppb of VOC, and a NO₂ sensitivity of 1.87 ppb MDA8 ozone per ppb NO₂. The ΔO₃ from the VOC perturbation is calculated from removal of VCP, and thus 2.68 is our estimate of the influence of VCP emissions on MDA8 ozone over the OLHO region on episode days.

Since both the VOC and NO₂ sensitivities are positive, the OLHO region is, on average, sensitive to both reductions in VOC and NO₂ concentrations. The

Table 2

Selected Concentration Differences and Sensitivities Calculated From Equations 1 and 2

Date	From VCP—no VCP		From NEI17m—NEI17	
	ΔO ₃	S _{VOC}	ΔO ₃	S _{NOx}
All 10 cases	2.68	0.78	1.01	1.87
June 2	5.90	0.76	0.37	0.23
June 3	2.70	0.58	0.96	1.99
June 4	1.75	0.62	1.92	6.06
June 9	1.43	0.81	1.10	4.38
June 10	2.08	0.67	2.21	12.04
June 11	2.23	1.37	1.64	23.01
June 12	2.32	0.74	1.01	1.97
June 14	1.01	0.92	2.06	30.1
June 15	3.26	0.79	1.42	1.47
June 16	3.00	1.81	−3.19	−13.09

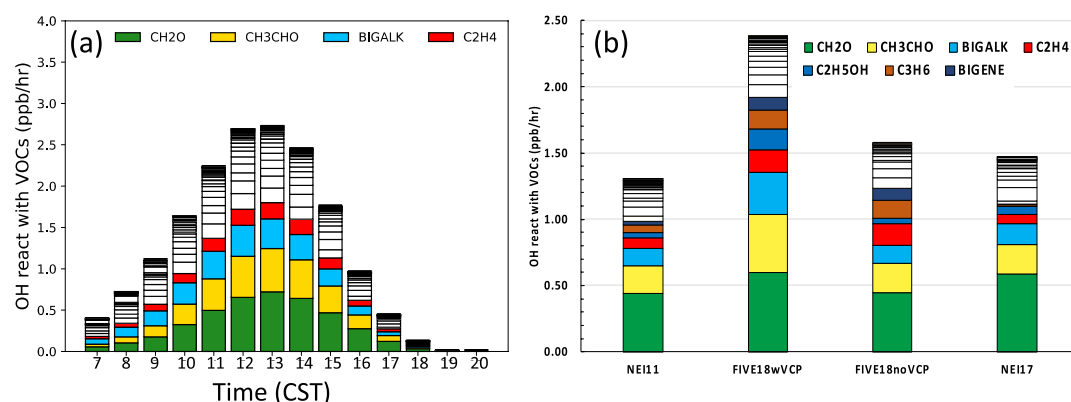


Figure 9. (a) Volatile organic compound (VOC) reactions OH (ppb/hr) by hour of day and Model for Ozone and Related chemical Tracers lumped for NEI14_wVCP simulation and OLHO region on 2 June. Formaldehyde (CH₂O), Acetaldehyde (CH₃CHO), BIGALK, and Ethylene (C₂H₄) are VOCs with the highest contribution to reactivity with OH. (b) VOC reactions with OH (ppb/hr) averaged from 1,000 to 1,400 on 2 June for all four simulations. Top VOC contributors are colored and labeled. VOC as OH reactivity (1/s) is 0.83, 1.28, 0.96, and 0.55 for NEI11, FIVE18_VCP, FIVE18_noVCP, and NEI17 respectively.

VOC sensitivities have relatively low variability, ranging from 0.58 ppb/ppb to 1.81 ppb/ppb. All are positive. On the other hand, the NO₂ sensitivities have much more variation, ranging from −13 to +30 ppb/ppb. Two days had particularly low sensitivities. June 2 had near zero NO_x sensitivity over the OLHO region during the time window (1000–1400 LST) used. June 16 had a negative NO₂ sensitivity, occurring in a geographically small OLHO offshore of Milwaukee and transected by a high NO₂ plume. In the NEI17m simulation used for the NO_x sensitivity, the peak hourly ozone increased by 2 ppb, but the spatially averaged MDA8 ozone decreased by 3 ppb, resulting in a negative sensitivity to the increase in NO_x emissions and NO₂ concentrations resulting from the emission perturbation. All other days showed positive sensitivity to NO₂ concentrations. The sensitivities are generally consistent with the independent methods and analysis reported in Acdan et al. (2020), where Lagrangian box model simulations were analyzed for sensitivity to emissions for June 2, 4, 11, 12, and 15. A more detailed comparison can be found in Table S5 in Supporting Information S1, but there is general agreement for 4 of the 5 days, and disagreement for June 4.

3.5. Insights From the Integrated Reaction Rate (IRR) Analysis

Formaldehyde (labeled as CH₂O in Figure 9) is the top contributor to the VOC reactivity during the daytime hours followed by acetaldehyde and BIGALK. Both formaldehyde and acetaldehyde can be emitted directly or form as a secondary pollutant from degradation of anthropogenic and biogenic VOCs (Luecken et al., 2012). FIVE18_VCP simulation has the highest mean VOC reactivity on 2 June over the OLHO region, while the other three inventories led to similar modeled VOC reactivities. In all four simulations formaldehyde is identified as the top VOC contributor to the reactivity with OH with the highest reactivity rate simulated for NEI17.

Vermeuel et al. (2019) identified formaldehyde, isoprene, and acetaldehyde as the top contributors to the reactivity with OH. Isoprene was not ranked as the top contributors in our analysis. This is likely due to the fact that Vermeuel reported the compounds contributing reactivity at the receptor site (on land, Zion, IL), where fresh isoprene was emitted into the parcel, and not at the point of highest net ozone formation over the lake as in this work.

The IRR was further used to derive the LRO_x/LNO_x ratio which serves as an indicator of the sensitivity of ozone production to NO_x and VOCs. Figure 10 shows the median of LRO_x/LNO_x ratio for all the days (1–19 June) and for the 10 high ozone days in FIVE18_VCP scenario averaged over 1000–1400 LST (panel a) and over 1300–1400 LST (panel b; corresponding to TROPOMI overpass time). Considering all days, both averaging times show that city of Chicago and the southwestern parts of the lake are VOC-sensitive (LRO_x/LNO_x < 0.35). Due to higher NO_x suppression earlier in the day, averaging from 1000 to 1400 LST (Figure 10a) yields a larger VOC-sensitive region than using only the TROPOMI overpass time (Figure 10b).

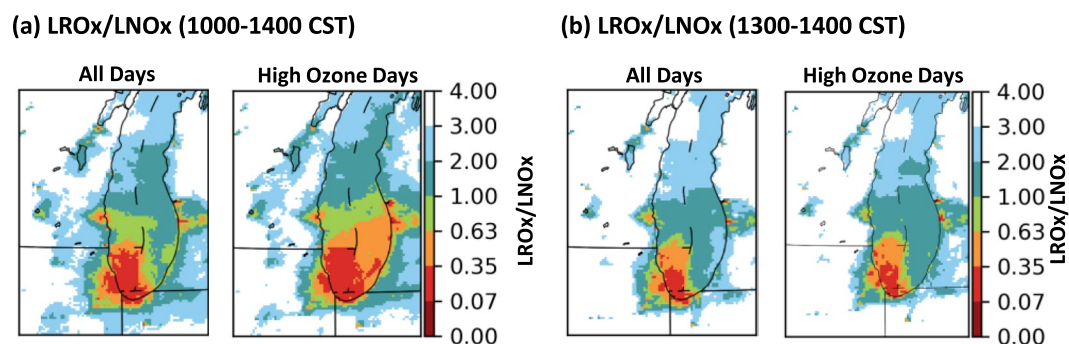


Figure 10. Median of the LRO_x/LNO_x ratio in the FIVE18_VCP scenario during all the days and high ozone days averaged over (a) 1000–1400 LST and (b) 1300–1400 LST.

Except for NO_x hotspots in Milwaukee, Muskegon, and Holland (see Figure 14 for locations), other coastal receptors are predominantly NO_x -sensitive based on the $LRO_x/LNO_x < 0.35$ criteria. Results for high ozone days suggest that portions of the city of Chicago remain in a VOC-sensitive regime.

Acidan et al. (2020) used FNR from TROPOMI to contrast VOC sensitivity on high ozone episode days relative to and ozone season (June–October) averages; and they concluded that the VOC-sensitive region decrease in size on episode days. Subsequent analysis by Acidan et al. (2020) showed that these differences arose due to including October in the ozone season composite. Figure 10a shows a larger VOC-sensitive region on episode days, when results are averaged over 1000–1400 LST. Figure 10b shows that the VOC-sensitive region on episode days changes only slightly when selecting the TROPOMI overpass time, which is consistent with the updated analysis of TROPOMI FNR using June–September for the ozone season composite. The VOC-sensitive region calculated by Koplitz et al. (2021) using 2016 emissions and CAMx higher order direct decoupled method is very similar to that of Figure 10b.

It is important to note that the chemical regime over the lake varies from day-to-day (as illustrated in Figure 8) depending on multiple factors. Figure S11 in Supporting Information S1 shows the spatial distribution of the LRO_x/LNO_x ratio for each high ozone day.

We further investigated whether the sensitivity ratios (a) LRO_x/LNO_x and (b) FNR are predictive of the more complex grid-cell specific changes in MDA8 ozone on high ozone days. We use the graphical technique as described in methods. In summary, brute force sensitivities to emissions are calculated from paired model runs and reduced to a grid-cell and day-specific angle α . See Figure 2 for more background. To review, α of 90° indicates NO_x -sensitive and VOC-insensitive (expected at high LRO_x/LNO_x and high FNR), 45° as NO_x -sensitive and VOC-sensitive, 0° as NO_x -insensitive and VOC-sensitive (expected at the transition point from NO_x -sensitive to VOC-sensitive conditions). Figure 11 shows that the expected behavior is born out. Warm colors in Figure 11

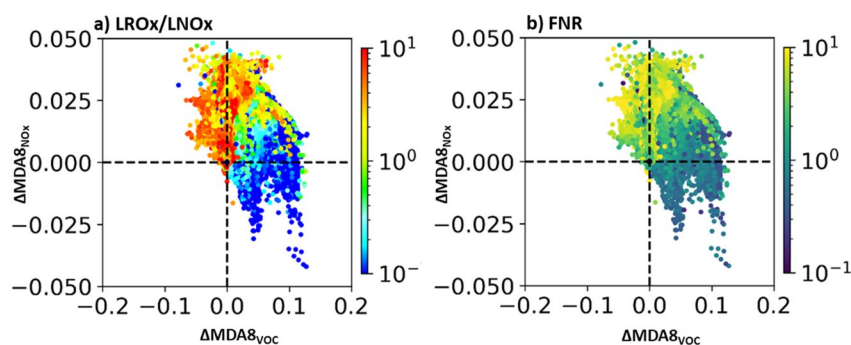


Figure 11. Examples showing qualitative predictive power of hour- and pixel-specific LRO_x/LNO_x and FNR ratios (color) to brute force sensitivities from photochemical grid model modeling with perturbed emissions (position on the plane). (a) Example using LRO_x/LNO_x for 1200 LST on 2 June and MDA8 on 2 June; (b) Example for the same hour with FNR within the boundary layer. Similar plots for P_{O_3} are in the Supporting Information S1.

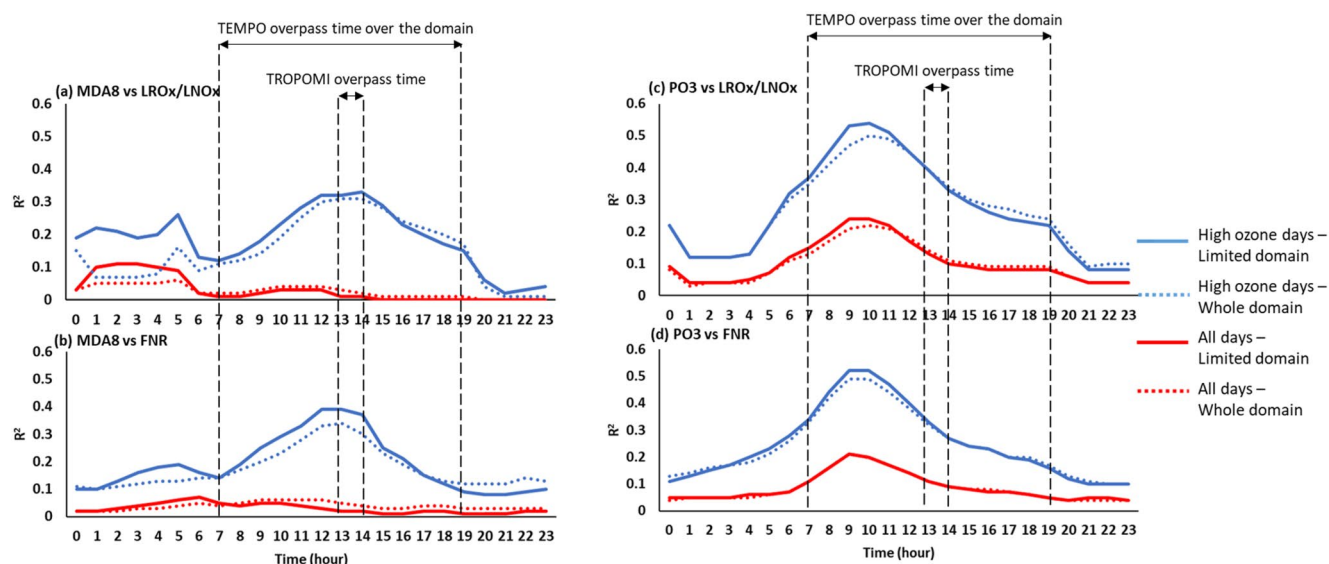


Figure 12. Correlation analysis to determine hour of day where local sensitivity variables are most predictive of brute-force sensitivity to anthropogenic volatile organic compound (VOC) and NO_x emission changes. (a) MDA8 versus $\text{LRO}_x/\text{LNO}_x$ (b) MDA8 versus FNR ratio, and (c) P_{O_3} versus $\text{LRO}_x/\text{LNO}_x$, and (d) P_{O_3} versus FNR ratio. Values of the angular parameter α between -22.5 and 112.5 considered. Limited domain refers to the domain shown in Figure 6. The actual and potential overpass time (over Midwest) for TROPOMI polar orbiting and TEMPO geostationary satellites are also shown, respectively.

show that the highest $\text{LRO}_x/\text{LNO}_x$ values correspond to α of 90° , where $\Delta\text{MDA8}_{\text{NO}_x} > 0$ and $\Delta\text{MDA8}_{\text{VOC}} \approx 0$. The lowest $\text{LRO}_x/\text{LNO}_x$ and FNR occur at $\alpha < 0$, or VOC-sensitive conditions, as expected. VOC sensitivity is nearly always positive. Samples of the correlation analysis between the sensitivity variables ($\text{LRO}_x/\text{LNO}_x$ and FNR) and α can be found in Figure S12 in Supporting Information S1. Nevertheless, we acknowledge that these ratios primarily are predictive of ozone production (Kleinman et al., 2001) rather than concentration. They will only be predictive of ozone concentrations to the extent that other drivers of concentration are small compared to net chemical production. We show this directly by investigating correlation of the angular parameter with P_{O_3} (Figure S13 in Supporting Information S1).

Results are shown in Figures 12a and 12b for MDA8 and in Figures 12c and 12d for P_{O_3} . The peak values for both P_{O_3} versus $\text{LRO}_x/\text{LNO}_x$ (panel c; blue lines) and P_{O_3} versus FNR (panel d; blue lines) are more than 0.5 and higher compared with MDA8 values (panels a, b). Furthermore, while MDA8 correlates with indicator ratios during high ozone days, it has very low correlation considering all the days (blue lines vs. red lines in panels a, b). These confirm that the correlation between P_{O_3} and indicator ratios are higher than the ones for MDA8. Nonetheless, considering only the 10 high ozone days in both analysis leads to higher correlations compared to the analysis done over all the days. However, the peak correlation values are still limited, indicative of other factors also be responsible for ΔMDA8 and $\Delta\text{P}_{\text{O}_3}$ in the tests. Changing the extent of the domain within the analysis had only a small effect on the results when considering multiple days, these are most likely due to the averaging many days in this analysis since this analysis for 2 June led to very high values (Figure S14 in Supporting Information S1). Similarly, Figure 13 shows the impact of averaging on P_{O_3} fractional changes. Specifically, 2 June was strongly a VOC-limited day and Figure 13d shows the decrease in net ozone production over the lake occurring from the 20% NO_x emissions increase. This behavior occurred at several urban locations throughout the domain on June 2. These features (decreases in P_{O_3} from the NO_x increase) are less prominent when averaging over the 10 high ozone days (panel f).

Figure 12 also shows the hourly values during the day. In P_{O_3} correlation plots in Figure 12 (panels c, d), we found the highest correlations for both $\text{LRO}_x/\text{LNO}_x$ and FNR ratios before noon (0900–1200 LST), which does not coincide with the TROPOMI overpass time (1300–1400 LST). On the other hand, peak correlations in MDA8 plots (panels a, b) during high ozone days overlap with TROPOMI overpass time. With the TEMPO Geostationary satellite mission launching in December 2022, hourly FNR can be retrieved during the day (0700–1900 over Midwest LST), which will help in validating these findings. Considering only the 10 high ozone days in

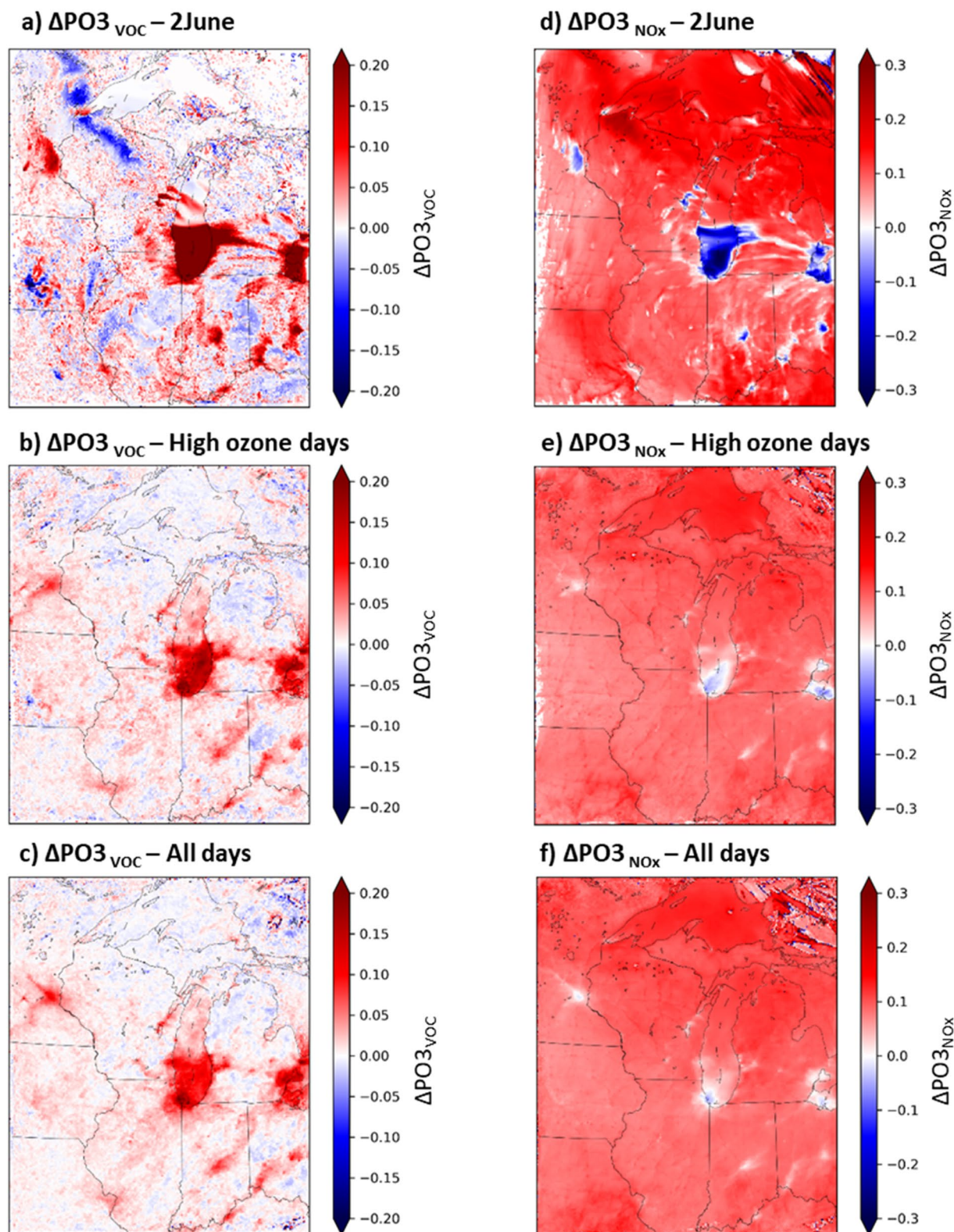


Figure 13. The fractional changes in P_{O_3} (ΔP_{O_3}) due to perturbation of anthropogenic volatile organic compound (VOC) (left column) and anthropogenic NO_x emissions (right column) for June 2 (top row), 10 high ozone days (middle row), and all the days in this work (bottom row). The blue colors show that P_{O_3} decreases by increasing emissions (i.e., disbenefit). VOC perturbation is inclusion of VCP relative to exclusion. NO_x perturbation is 20% increase relative to the NEI17 case. Figures S15 and S16 in Supporting Information S1 show net ozone production and MDA8 concentrations for June 2 and the 10 high ozone days from four inventories, respectively.

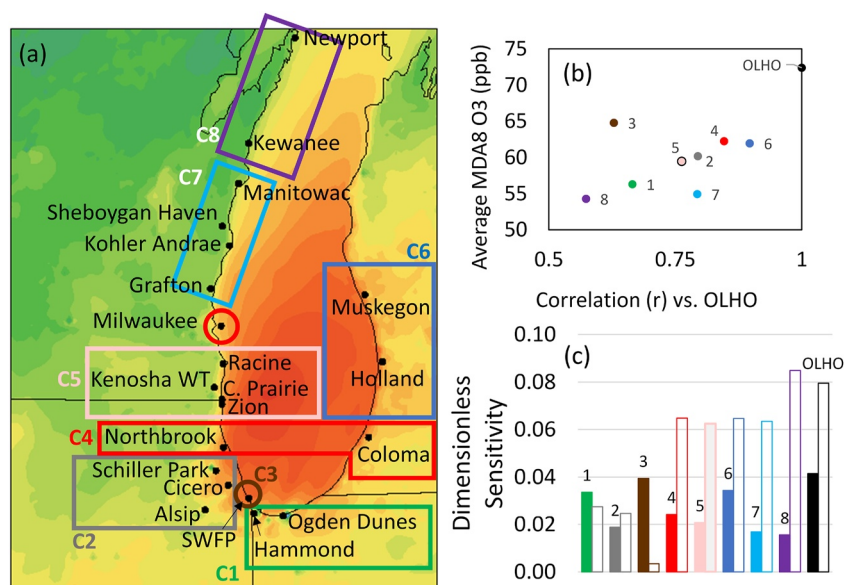


Figure 14. Cluster analysis of ozone sensitivity at selected sites around Lake Michigan over a background of modeled MDA8 ozone. (a) Sites organized into clusters according to similarity in day-specific and inventory-specific MDA8 ozone on high ozone days. (b) Average MDA8 ozone of each cluster (y-axis) and correlation coefficient with over-lake high ozone (OLHO) grid cells (x-axis), whose MDA8 ozone averaged 72.4 ppb. (c) Dimensionless emission sensitivity of ozone in each cluster to anthropogenic volatile organic compound changes (solid) and anthropogenic NO_x changes (open) bars.

the analysis leads to higher correlations compared to the analysis done over all the days. Moreover, changing the extent of the domain within the analysis had only a small effects on the results.

3.6. Relating the Over-Lake High Ozone to Shoreline and Near-Coastal Receptor Sites

The 21 receptor sites (routine air quality monitors historically relevant to ozone air quality planning) had MDA8 ozone values which ranged from the lowest values of 53.9 ppb at the northernmost site of Newport, to the highest value of 68.9 ppb at the Chiwaukee Prairie site on the LMOS ozone episode days. The sites are mapped in Figure 14. Observed and modeled MDA8 ozone at these sites can be found in Table S4 in Supporting Information S1.

We grouped the different sites into clusters using k-means cluster analysis based on similarity in modeled ozone concentrations and in response to changes in emissions (see methods). Figure 14a shows the result of the cluster analysis. Clusters have similar modeled ozone concentrations and respond similarly to the variations in emissions within the four inventories. Figure 14b places the clusters according to MDA8 ozone concentration on high ozone days, and correlation coefficients with respect to OLHO MDA8 ozone. Clusters are numbered in a generally south-to-north order.

Clusters 2, 4, 5, 6, and 7 were all (in the model) correlated with the OLHO ozone with a correlation coefficient exceeding 0.75. This consisted of all the receptor sites from Manitowac in the north to the Chicago metro area in the site, with the notable exception of some high NO_x urban and industrial sites near the southern end of Lake Michigan (clusters 1 and 3). The South Water Filtration Plant site was consistently placed in a cluster of its own, and this behavior was independent of the total number of clusters used in k-means (it occurred whether 5, 6, 7 or 8 total clusters were used).

Cluster 6 (eastern shore of the lake, in western Michigan) had the highest correlation with OLHO ozone. The five Cook county sites that we included in the analysis, representing the high emission core of the Chicago metro area, was split into three clusters by the k-means algorithm. South Water Filtration Plant was placed by itself as a high ozone site, with relatively low correlation to the OLHO area, the highest dimensionless VOC sensitivity of all the clusters, and the lowest NO_x sensitivity of all the clusters. Together with cluster 1 in northern Indiana, these are the only sites with higher dimensionless VOC sensitivity than their dimensionless NO_x sensitivity. In

order of increasing sensitivity to NO_x emissions perturbation were cluster 2, representing Cook county sites not directly on the lake, and cluster 4, which included Northbrook in Cook county, as well as Coloma on the eastern shore of the lake, and Milwaukee. As Figure 4 shows, the sites of cluster 4 have relatively high NO_x concentration compared to sites to the south of Milwaukee (cluster 5) and to the north of Milwaukee (cluster 7).

Cluster 7 includes coastal Wisconsin sites north of Milwaukee. This cluster has lower modeled ozone concentrations, due to less frequent lake breeze impact. As shown in Abdi-Oskouei et al. (2020) and Stanier et al. (2021), the WRF-Chem model sometimes failed to form a lake breeze that comes onshore in areas of clusters 3 and 5 accurately. Thus, the true ozone sensitivity for cluster Sheboygan and surrounding cluster 7 sites may be closer to the OLHO sensitivity due to the insufficient modeled transport from OLHO to cluster 7 receptors. Cluster 8 consists of the northernmost sites, which have low MDA8 ozone and low correlation with ozone in the OLHO region. With the exception of cluster 8, all sites had lower dimensionless NO_x sensitivity than the OLHO region, likely due to a combination of higher influence from upwind overland ozone concentrations relative to the lake, as well as to high localized NO_x concentrations.

Solid bars in 4c graph the dimensionless emissions sensitivity of MDA8 ozone to an anthropogenic VOC emission perturbation. These are calculated from the FIVE18_VCP—FIVE18_noVCP simulations (see methods). Open bars graph the dimensionless emissions sensitivity of MDA8 ozone to an anthropogenic NO_x emission perturbation, calculated from the NEI17 and NEI17m simulations (see methods). A dimensionless emissions sensitivity of 0.1 means that a 10% increase (decrease) in emissions yields a 1% increase (decrease) in ozone concentrations. As a reference, the OLHO region is sensitive to both VOC (solid) and NO_x (open) changes, with numerical values of 0.04 and 0.08, respectively.

We acknowledge that our dimensionless VOC emissions sensitivities are calculated from large perturbations (see Figure 2 for the sizes of the perturbations) and accordingly, are subject to uncertainties. Furthermore, our analysis is for June 2017 only, and may not be representative for other months of the ozone season. As shown in Figure 8, and in Table 2, variations in the emissions sensitivity are strong between episode days.

Clusters that are qualitatively similar to the OLHO area (NO_x sensitivity > 0.06 , NO_x sensitivity $>$ VOC sensitivity) include clusters 4–8, consisting of all sites from Northbrook and farther north. Sites south of that (clusters 1–3) had lower dimensionless NO_x -sensitivity. We hypothesize that the high OLHO anthropogenic VOC sensitivity (compared to the coastal receptor sites) is due to the lower biogenic VOC influence over the lake, and higher biogenic VOC influence over land.

Kopplitz et al. (2021) also investigated sensitivity at sites located in the Chicago airshed, which intersect with sites in clusters 1 to 4 in our work. For high ozone days, all sites were classified (using 2016 modeling) as near the isopleth ridgeline or somewhat NO_x -sensitive. Day-of-week analysis gave a similar result. Thus Kopplitz et al. (2021) sensitivities are qualitatively similar to those of Figure 14c for clusters 1 to 4. Figures 6 and 10 show very sharp gradients in sensitivity regime near the southern shore of Lake Michigan, at the Illinois Indiana border. The VOC-sensitive zone extends approximately one grid cell onshore (~ 4 km), and the sites analyzed in this work in the northwestern Indiana cluster were one and four km away from the lakeshore, respectively. A number of challenging features complicate model-based and observational determination of sensitivity here, including monitor locations relative to lakeside point sources (and grid cell boundaries), model resolution, plume-in-grid effects for large point sources, spatiotemporal assignment of nearshore shipping and recreational boating emissions, and mixing of elevated NO_x emissions to the surface. Observational analysis may be complicated by operational schedules of industrial sites, shipping operations, and freight rail that may not fit usual day-of-week patterns.

Using 2017–2019 ozone design values based on observations, we find that clusters 2–7 each contain 1 or more monitors that exceed the 70 ppb National Ambient Air Quality Standard (NAAQS) ozone standard by 3 ppb (cluster 3), 4 ppb (clusters 4 and 6) or 5 ppb (clusters 2, 5, and 7). Using the cluster-specific NO_x and VOC sensitivities, approximate magnitudes of anthropogenic VOC and NO_x emissions reductions that will achieve the NAAQS can be calculated for each cluster. The magnitudes of required emissions reduction are large, given that up to a 5 ppb ozone reduction is required (6.7%). But even at the highest fractional sensitivity in any of those clusters in Figure 14 (0.065), a 10% emission reduction only results in a 0.65% ozone decrease—much less than the 6.7% decrease needed.

Using linear sensitivities in this way has obvious limitations, including the fact that sensitivity at each monitor is different (and is not represented by the cluster average), the true sensitivities are nonlinear, the 10 days in June

2017 have limits in their representation of NAAQS exceedances in general, and the spatial patterns of emission changes may differ from those assumed here. Furthermore, as anthropogenic NO_x and VOC emissions decrease due to technology trends (e.g., renewable electricity and electrification of transportation), concentrations of ozone and ozone precursors outside of our modeling domain will likely decrease, decreasing the amount of reduction required from within the domain. An exception to this trend is the uncertainty in soil NO_x emissions. On average, soil emissions of NO_x account for 15% of the global NO_x emissions (Hudman et al., 2012; Weng et al., 2020). Emissions are highly variable with peak emissions during spring and summer crop fertilization and accounting for fertilization management improved modeled NO_2 and increased surface ozone concentrations (Oikawa et al., 2015). The version of MEGAN biogenic emissions used in this work does not consider fertilization events. As large agricultural areas border the Lake Michigan airshed, increases in soil NO_x emissions may run counter to anthropogenic emissions decreases.

4. Implications and Summary

We have shown that the ozone hotspot that forms over southern Lake Michigan during summertime ozone episodes in the Lake Michigan region, has, on average, positive sensitivity to NO_2 concentrations, total VOC concentrations, anthropogenic NO_x emissions, and anthropogenic VOC emissions. During the 10 episode days in June 2017, the sensitivity in the OLHO region to VOCs was always positive, and averaged 0.78 ppb MDA8 ozone per ppb VOC. Relative to fractional changes in anthropogenic emissions, the fractional sensitivity of episode day MDA8 ozone was 0.04, implying a 10% decrease in VOC emissions would, on average, lower MDA8 ozone over the lake by 0.4%, or 0.3 ppb.

Sensitivity to NO_x was lower than the average sensitivity on two of the 10 days. This included the June 2 episode, with approximately zero NO_x sensitivity, indicating VOC-sensitive ozone in the OLHO area on June 2. And it included June 16, with a negative NO_x sensitivity. Considering all 10 days, the average NO_2 sensitivity was 1.87 ppb MDA8 ozone per ppb of NO_2 . Dimensionless sensitivity of episode day MDA8 ozone to anthropogenic NO_x emissions was 0.08. In other words, a 10% decrease in NO_x emissions would, on average, lower MDA8 ozone in the OLHO region by 0.8% (or ~ 0.6 ppb) on episode days.

The pattern of positive VOC sensitivity (on all days) and positive NO_x sensitivity (on the majority of days) matches results from Vermeuel et al. (2019) and the extension of that work in Acdan et al. (2020). It is notable that the most analyzed day of the LMOS 2017 field campaign, 2 June, was an atypical day with VOC-sensitive ozone along the trajectory to Zion, IL (as shown by Vermeuel et al. (2019) and Acdan et al. (2020)). This corresponds to near zero sensitivity of ozone to NO_2 concentration in this work. This was for the OLHO on June 2, which was located in the southwest corner of Lake Michigan, including the area directly offshore from Zion.

We believe that this ozone hotspot has a strong influence on coastal monitors, particularly in the southern portion of Lake Michigan. Cluster analysis of 21 policy-relevant ozone monitoring sites identified eight clusters according to their MDA8 ozone concentration on episode days, the temporal variation of MDA8 ozone, and the sensitivity of MDA8 ozone to emission perturbations. Five of the eight clusters have their MDA8 ozone behavior (temporal variability and sensitivity to emissions) correlated with that of the OLHO region with correlation coefficient of higher than 0.75. Accordingly, coastal locations will benefit from ozone reductions in the OLHO region; however, they are further influenced by local titration by nearby NO emissions, local production of ozone, and the influence of rural continental air, and by entrainment of ozone (usually lower ozone) in air from aloft.

We further show that the likely influence of VCP on ozone in the region is 2.68 ppb (MDA8 ozone on high ozone days) in the center of the over-lake ozone hotspot. An alternate quantification of the effect on MDA8 ozone is from Figure 6d, which has a peak value of 2.1 ppb (averaged over the episode days). This sensitivity is lower than that found for Los Angeles (9 ppb, (Qin et al., 2021)), presumably because of the higher biogenic VOC background over Lake Michigan during summer. Another modeling study found an effect size ranging from 5 to 12 pb downwind of New York City (Coggon et al., 2021).

The spatial pattern in the sensitivities is corroborated by mapping the $\text{LRO}_x/\text{LNO}_x$ ratio over the lake. The majority of the region is estimated as NO_x sensitive, and the spatial extent of the VOC sensitive region depends on the time of day. Using 1000–1400 LST, the VOC sensitive region on high episode days is limited to a few high NO_x emission locations (Chicago IL, northern Indiana, Milwaukee WI, Muskegon MI, and Holland MI) and the southwestern quadrant of Lake Michigan (west of 86.87°W and south of 42.50°N). Using the hours of the TROPOMI

overpass time, the VOC sensitive region is smaller, as VOC sensitivity evolves over the lake from highest values in the morning, to lower values throughout the rest of the day.

As shown in our previous work, which included a thorough comparison of aircraft vertical ozone profiles in Figure 2 of Abdi-Oskouei et al. (2020) and Figure 6 of Stanier et al. (2021), the WRF-Chem model often fails to produce sufficiently high ozone concentrations on episode days, particularly over water and at altitude below 1.5 km. One likely contributing factor for this is insufficient VOC and NO_x concentrations on the days and in the grid cells and vertical layers in question. A second problem with PGM, is that they may make sufficient ozone in the reactive plume over the lake, but then fail to transport it in a skillful way to achieve a match with observations. This, for example, has been discussed for June 11 in Abdi-Oskouei et al. (2020) and June 12 in Stanier et al. (2021). The technique employed in this paper, where we focus on over the lake high ozone area (regardless of whether it is in an accurate location) helps moderate the influence of this second type of error.

Taken as a whole, we believe that a major implication of our work is to show that large portions of the Lake Michigan airshed contains a mix of NO_x -sensitive and VOC-sensitive areas on high ozone days on average. Ozone concentrations in these areas will decrease in response to reductions in NO_x and/or VOC emissions. Our work indicates that the dimensionless sensitivity to anthropogenic NO_x emissions reduction is greater than that of anthropogenic VOC reductions (on a molar basis, excluding methane). In other words, equal percentage reductions in anthropogenic NO_x emissions, and in anthropogenic VOC emissions, do not yield equal air quality benefits—the benefit is greater for NO_x emission reductions. However, ozone formation contributions vary by hydrocarbon species, and additional work could identify species where reductions would be most effective.

Our modeling indicates a significant area (Figure 10) that is VOC-sensitive on average. This area is decreasing over time due to reductions in NO_x emissions; additional investigation of the existence of VOC-sensitive regions and monitors around Chicago and in northern Indiana, especially through observational methods, is still needed. A minority of episode days (e.g., 2 June 2017) may be significantly more VOC-sensitive than NO_x -sensitive for a significant portion of the domain, including at monitor locations that are on average, NO_x -sensitive. Transitional behavior (low responsiveness of O_3 to NO_x reductions, or limited increases in ozone as NO_x is reduced) will occur, and can be counteracted by simultaneous reductions in VOCs.

We believe this work strengthens the conceptual model of ozone formation in the Lake Michigan airshed, characterized by ozone formation in a shallow layer over the Lake, followed by onshore transport. Decreases in NO_2 and VOC in this formation region over the lake should correlate with ozone improvements at lakeshore monitors. Remote and in situ monitoring of key indicators such as NO_2 and FNR over southern Lake Michigan are likely to shed considerable light on the changing ozone formation regimes over the region. Similar insight can be drawn from data at coastal monitor locations, especially if measurements are of high time resolution, such that lake breeze chemical conditions can be analyzed segregated from land-dominated air parcels. The latest generation of polar orbiting satellites for air quality, and the anticipated geostationary satellites, are likely to be very useful for monitoring ozone precursors.

Data Availability Statement

Ground-based measurements were download from the EPA Air Data website: https://aqs.epa.gov/aqsweb/airdata/download_files.html. A reduced version of WRF-Chem outputs is available from <https://doi.org/10.25820/data.006193>.

References

- Abdi-Oskouei, M., Adelman, Z., Al-saadi, J., Bertram, T., Carmichael, G., Christiansen, M., et al. (2019). 2017 Lake Michigan Ozone Study (LMOS) preliminary finding report. Retrieved from https://www.ladco.org/wp-content/uploads/Research/LMOS2017/LMOS_LADCO_report_revision_apr2019_final.pdf
- Abdi-Oskouei, M., Carmichael, G., Christiansen, M., Ferrada, G., Roozitalab, B., Sobhani, N., et al. (2020). Sensitivity of meteorological skill to selection of WRF-Chem physical parameterizations and impact on ozone prediction during the Lake Michigan Ozone Study (LMOS). *Journal of Geophysical Research: Atmospheres*, 125(5), 1–25. <https://doi.org/10.1029/2019JD031971>
- Abdi-Oskouei, M., Roozitalab, B., Stanier, C., & Carmichael, G. (2022). WRF-Chem model outputs to study the impact of Volatile Chemical Products, Other VOCs, and NO_x on Peak Ozone in the Lake Michigan Region during June 2017. <https://doi.org/10.25820/data.006193>
- Acidan, J., Vermeuel, M., Bertram, T. H., & Pierce, R. B. (2020). Observation-based analyses of the sensitivity of ozone formation in the Lake Michigan region to NO . Retrieved from https://www.ladco.org/wp-content/uploads/Projects/Ozone/2020_WI-DNR_OBM_Analysis/LADCO_FinalReport_2020.pdf

Acknowledgments

The authors would like to acknowledge LMOS 2017 science team. The National Center for Atmospheric Research is sponsored by the National Science Foundation. We would like to thank Dr. Stuart McKeen, and Dr. Kirk Baker for providing FIVE18 and NEI17 emission inventories. This work was funded in part by the National Science Foundation under collaborative Grant AGS-1712909. We acknowledge EPA and the NOAA GOES-R program office for supporting the measurements at Sheboygan, and the Electric Power Research Institute (EPRI) for supporting the Scientific Aviation airborne measurements. The University of Iowa modeling team acknowledges the Atmospheric Composition Modeling and Analysis Program grant (award # 80NSSC19K0946). Any opinions, findings, and conclusions or recommendations expressed in this material are those of the author(s) and do not necessarily reflect the views of the National Science Foundation nor should they be construed as an official National Oceanic and Atmospheric Administration or U.S. Government position, policy, or decision. The views expressed in this paper are those of the authors and do not necessarily represent the views or policies of the U.S. Environmental Protection Agency. EPA does not endorse any products or commercial services mentioned in this publication.

- Atmospheric Chemistry Observation & Modeling (ACOM). (2021). Photolysis in WRF-Chem. Retrieved from https://www2.acom.ucar.edu/sites/default/files/wrf-chem/Instructions_photolysis_opt_4.pdf
- Cleary, P. A., Fuhrman, N., Schulz, L., Schafer, J., Fillingham, J., Bootsma, H., et al. (2015). Ozone distributions over southern Lake Michigan: Comparisons between ferry-based observations, shoreline-based DOAS observations and model forecasts. *Atmospheric Chemistry and Physics*, 15(9), 5109–5122. <https://doi.org/10.5194/acp-15-5109-2015>
- Coggon, M. M., Gkatzelis, G. I., McDonald, B. C., Gilman, J. B., Schwantes, R. H., Abuhassan, N., et al. (2021). Volatile chemical product emissions enhance ozone and modulate urban chemistry. *Proceedings of the National Academy of Sciences of the United States of America*, 118(32), e2026653118. <https://doi.org/10.1073/pnas.2026653118>
- Doak, A. G., Christiansen, M. B., Alwe, H. D., Bertram, T. H., Carmichael, G., Cleary, P., et al. (2021). Characterization of ground-based atmospheric pollution and meteorology sampling stations during the Lake Michigan Ozone Study 2017. *Journal of the Air and Waste Management Association*, 71(7), 866–889. <https://doi.org/10.1080/10962247.2021.1900000>
- Duncan, B. N., Yoshida, Y., Olson, J. R., Sillman, S., Martin, R. V., Lamsal, L., et al. (2010). Application of OMI observations to a space-based indicator of NOx and VOC controls on surface ozone formation. *Atmospheric Environment*, 44(18), 2213–2223. <https://doi.org/10.1016/j.atmosenv.2010.03.010>
- Dye, T. S., Robert, P. T., & Korc, M. E. (1995). Observations of transport processes for ozone and ozone precursors during the 1991 Lake Michigan Ozone Study. *Journal of Applied Meteorology*, 34(8), 1877–1889. [https://doi.org/10.1175/1520-0450\(1995\)034<1877:oofpo>2.0.co;2](https://doi.org/10.1175/1520-0450(1995)034<1877:oofpo>2.0.co;2)
- Emery, C., Liu, Z., Russell, A. G., Odman, M. T., Yarwood, G., & Kumar, N. (2016). Recommendations on statistics and benchmarks to assess photochemical model performance. *Journal of the Air and Waste Management Association*, 67(5), 582–598. <https://doi.org/10.1080/10962247.2016.1265027>
- Emmons, L. K., Walters, S., Hess, P. G., Lamarque, J. F., Pfister, G. G., Fillmore, D., et al. (2010). Model development description and evaluation of the model for ozone and related chemical tracers, Version 4 (MOZART-4) (pp. 43–67).
- Foley, T., Betterton, E. A., Jacko, R., & Hillery, J. (2011). Lake Michigan air quality: The 1994–2003 LADCO aircraft project (LAP). *Atmospheric Environment*, 45(18), 3192–3202. <https://doi.org/10.1016/j.atmosenv.2011.02.033>
- Francoeur, McDonald, B. C., Gilman, J. B., Zarzana, K. J., Dix, B., Brown, S. S., et al. (2021). *Quantifying methane and ozone precursor emissions from oil and gas production regions across the contiguous US*. Environmental Science & Technology.
- Gkatzelis, G. I., Georgios, I., McDonald, B. C., Peischl, J., Aikin, K. C., Gilman, J. B., et al. (2021). Identifying volatile chemical product tracer compounds in U.S. cities. *Environmental Science and Technology*, 55(1), 188–199. <https://doi.org/10.1021/acs.est.0c05467>
- Grell, G. A., Peckham, S. E., Schmitz, R., McKeen, S. A., Frost, G., Skamarock, W. C., & Eder, B. (2005). Fully coupled “online” chemistry within the WRF model. *Atmospheric Environment*, 39(37), 6957–6975. <https://doi.org/10.1016/j.atmosenv.2005.04.027>
- Guenther, A., Karl, T., Harley, P., Wiedinmyer, C., Palmer, P. I., & Geron, C. (2006). Estimates of global terrestrial isoprene emissions using MEGAN (model of emissions of gases and aerosols from nature). *Atmospheric Chemistry and Physics*, 6(11), 3181–3210. <https://doi.org/10.5194/acp-6-3181-2006>
- Hodzic, A., & Jimenez, J. L. (2011). Modeling anthropogenically controlled secondary organic aerosols in a megacity: A simplified framework for global and climate models. *Geoscientific Model Development*, 4(4), 901–917. <https://doi.org/10.5194/gmd-4-901-2011>
- Hodzic, A., Madronich, S., Kasibhatla, P. S., Tyndall, G., Aumont, B., Jimenez, J. L., et al. (2015). Organic photolysis reactions in tropospheric aerosols: Effect on secondary organic aerosol formation and lifetime. *Atmospheric Chemistry and Physics*, 15(16), 9253–9269. <https://doi.org/10.5194/acp-15-9253-2015>
- Hoesly, R. M., Smith, S. J., Feng, L., Klimont, Z., Janssens-Maenhout, G., Pitkanen, T., et al. (2016). Historical (1750–2014) anthropogenic emissions of reactive gases and aerosols from the community emissions data system (CEDS) (Vol. 7).
- Hudman, R. C., Moore, N. E., Mebust, A. K., Martin, R. V., Russell, A. R., Valin, L. C., & Cohen, R. C. (2012). Steps towards a mechanistic model of global soil nitric oxide emissions: Implementation and space based-constraints. *Atmospheric Chemistry and Physics*, 12(16), 7779–7795. <https://doi.org/10.5194/acp-12-7779-2012>
- Inness, A., Baier, F., Benedetti, A., Bouarar, I., Chabrilat, S., Clark, H., et al. (2013). The MACC reanalysis: An 8 yr data set of atmospheric composition. *Atmospheric Chemistry and Physics*, 13(8), 4073–4109. <https://doi.org/10.5194/acp-13-4073-2013>
- Jeffries, H. E., & Tonnesen, S. (1994). A comparison of two photochemical reaction mechanisms using mass balance and process analysis. *Atmospheric Environment*, 28(18), 2991–3003. [https://doi.org/10.1016/1352-2310\(94\)90345-x](https://doi.org/10.1016/1352-2310(94)90345-x)
- Jin, X., Fiore, A. M., Murray, L. T., Valin, L. C., Lamsal, L. N., Duncan, B., et al. (2017). Evaluating a space-based indicator of surface ozone-NOx-VOC sensitivity over midlatitude source regions and application to decadal trends. *Journal of Geophysical Research: Atmospheres*, 122(19), 10439–10461. <https://doi.org/10.1002/2017jd026720>
- Kleinman, L. I., Daum, P. H., Lee, Y. N., Nunnermacker, L. J., Springston, S. R., Weinstein-Lloyd, J., & Rudolph, J. (2001). Sensitivity of ozone production rate to ozone precursors. *Geophysical Research Letters*, 28(15), 2903–2906. <https://doi.org/10.1029/2000gl012597>
- Knote, C., Hodzic, A., Jimenez, J. L., Volkamer, R., Orlando, J. J., Baidar, S., et al. (2014). 14 atmospheric chemistry and physics simulation of semi-explicit mechanisms of SOA formation from glyoxal in aerosol in a 3-D model.
- Kopplitz, S., Simon, H., Henderson, B., Liljegren, J., Tonnesen, G., Whitehill, A., & Wells, B. (2021). *Changes in ozone chemical sensitivity in the United States from 2007 to 2016*. ACS Environmental Au.
- Lake Michigan Air Directors Consortium. (2018). Interstate transport modeling for the 2015 ozone national ambient air quality standard. Retrieved from https://www.ladco.org/wp-content/uploads/Documents/Reports/TSDs/O3/LADCO_2015O3SIP_TSD_13Aug2018.pdf
- Li, M., McDonald, B. C., McKeen, S. A., Eskes, H., Levelt, P., Francoeur, C., et al. (2021). Assessment of updated fuel-based emissions inventories over the contiguous United States Using TROPOMI NO2 retrievals. *Journal of Geophysical Research: Atmospheres*, 126(24), 1–21. <https://doi.org/10.1029/2021jd035484>
- Lueken, D. J., Hutzell, W. T., Strum, M. L., & Pouliot, G. A. (2012). Regional sources of atmospheric formaldehyde and acetaldehyde, and implications for atmospheric modeling. *Atmospheric Environment*, 47(2), 477–490. <https://doi.org/10.1016/j.atmosenv.2011.10.005>
- Marvin, M. R., Roberts, S. J., Travis, K. R., & Liao, J. (2016). The framework for 0-D atmospheric modeling (FOAM) v3.1. *Geoscientific Model Development*, 9(9), 3309–3319. <https://doi.org/10.5194/gmd-9-3309-2016>
- McDonald, B. C., de Gouw, J. A., Gilman, J. B., Jathar, S. H., Akherati, A., Cappa, C. D., et al. (2018b). Volatile chemical products emerging as largest petrochemical source of urban organic emissions. *Science*, 359(6377), 760–764. <http://www.sciencemag.org/lookup/doi/10.1126/science.aag0524>
- McDonald, B. C., McKeen, S. A., Cui, Y. Y., Ahmadvor, R., Kim, S. W., Frost, G. J., et al. (2018a). Modeling ozone in the eastern U.S. using a fuel-based mobile source emissions inventory. *Environmental Science and Technology*, 52(13), 7360–7370. <https://doi.org/10.1021/acs.est.8b00778>
- Oikawa, P. Y., Ge, C., Wang, J., Eberwein, J. R., Liang, L. L., Allsman, L. A., et al. (2015). Unusually high soil nitrogen oxide emissions influence air quality in a high-temperature agricultural region. *Nature Communications*, 6(1), 8753. <https://doi.org/10.1038/ncomms9753>

- Pfister, G., Wang, C., Barth, M., Flocke, F., Vizuete, W., & Walters, S. (2019). Chemical characteristics and ozone production in the northern Colorado front range. *Journal of Geophysical Research: Atmospheres*, 124(23), 13397–13419. <https://doi.org/10.1029/2019jd030544>
- Pusede, S. E., & Cohen, R. C. (2012). On the observed response of ozone to NO_x and VOC reactivity reductions in San Joaquin valley California 1995–present. *Atmospheric Chemistry and Physics*, 12(18), 8323–8339. <https://doi.org/10.5194/acp-12-8323-2012>
- Qin, M., Murphy, B. N., Isaacs, K. K., McDonald, B. C., Lu, Q., McKeen, S. A., et al. (2021). Criteria pollutant impacts of volatile chemical products informed by near-field modelling. *Nature Sustainability*, 4(2), 129–137. <https://doi.org/10.1038/s41893-020-00614-1>
- Qin, M., Yu, H., Hu, Y., Russell, A. G., Odman, M. T., Doty, K., et al. (2019). Improving ozone simulations in the great lakes region: The role of emissions, chemistry, and dry deposition. *Atmospheric Environment*, 202, 167–179. <https://doi.org/10.1016/j.atmosenv.2019.01.025>. <https://www.sciencedirect.com/science/article/pii/S1352231019300470>
- Schroeder, J. R., Crawford, J. H., Fried, A., Walega, J., Weinheimer, A., Wisthaler, A., et al. (2017). New insights into the column CH₂O/NO₂ ratio as an indicator of near-surface ozone sensitivity. *Journal of Geophysical Research: Atmospheres*, 122(16), 8885–8907. <https://doi.org/10.1002/2017jd026781>
- Sillman, S. (1995). The use of NO_y, H₂O₂, and HNO₃ as indicators for ozone–NO_x–hydrocarbon sensitivity in urban locations. *Journal of Geophysical Research*, 100(D7), 14175–14188. <https://doi.org/10.1029/94JD02953>
- Skamarock, W. C., Klemp, J. B., Dudhia, J., Gill, D. O., Barker, D. M., Wang, W., & Powers, J. G. (2008). A description of the advanced research WRF version 3. NCAR Technical note NCAR/TN-4751STR.
- Stanier, Pierce, R. B., Abdi-Oskouei, M., Adelman, Z. E., Al-Saadi, J., Alwe, H. D., et al. (2021). Overview of the Lake Michigan ozone study 2017. *Bulletin of the American Meteorological Society*, 1–47.
- United States Environmental Protection Agency (U. S. EPA). (2021). Nonattainment areas for criteria pollutants (green book) Retrieved from <https://www.epa.gov/green-book>
- Vassilvitskii, S., & Arthur, D. (2006). K-Means++: The advantages of careful seeding. In *Proceedings of the eighteenth annual ACM-SIAM symposium on discrete algorithms*.
- Vermeuel, M. P., Novak, G. A., Alwe, H. D., Hughes, D. D., Kaleel, R., Dickens, A. F., et al. (2019). Sensitivity of ozone production to NO_x and VOC along the lake Michigan coastline. *Journal of Geophysical Research: Atmospheres*, 124(20), 10989–11006. <https://doi.org/10.1029/2019jd030842>
- Weng, H., Lin, J., Martin, R., Millet, D. B., Jaegle, L., Ridley, D., et al. (2020). Global high-resolution emissions of soil NO_x, sea salt aerosols, and biogenic volatile organic compounds. *Scientific Data*, 7(1), 1–15. <https://doi.org/10.1038/s41597-020-0488-5>
- Benjamin, S. G., Weygandt, S. S., Brown, J. M., Hu, M., Alexander, C. R., Smirnova, T. G., et al. (2016). A North American hourly assimilation and model forecast cycle: The rapid refresh. *Monthly Weather Review*, 144(4), 1669–1694. <http://journals.ametsoc.org/doi/10.1175/MWR-D-15-0242.1>
- Wisconsin Department of Natural Resources. (2021). Wisconsin air quality trends report. Retrieved from <https://dnr.wi.gov/files/PDF/pubs/am/AM583.pdf>
- Zaveri, R. A., Easter, R. C., Fast, J. D., & Peters, L. K. (2008). Model for simulating aerosol interactions and chemistry (MOSAIC). *Journal of Geophysical Research*, 113(13), 1–29. <https://doi.org/10.1029/2007jd008782>